



# Chapter 7

## Perovskite-coated gratings

Despite their structural simplicity, 1D grating samples can sustain many electromagnetic modes, from diffractive interference effects to more localised and waveguided modes. In plasmonic gratings we can distinguish between such ‘photonic’ gratings modes and the ‘plasmonic’ modes that involve interactions with excited surface plasmon polaritons (SPPs), as described in Sec. 3.2. The dispersion and efficiency of grating modes in optical spectra depend on the coupling with incoming/outgoing photons, and is very sensitive to factors such as the polarisation of light, changes in geometry and the refractive index of any coating materials.

In this Chapter the optical behaviour of perovskite-coated 1D gratings are explored, and CHPI-coated Ag gratings are used to understand the interactions between excitons and SPPs.

### 7.1 Experimental methods

The fabrication of dielectric-coated metal gratings is shown in Fig. 7.1(a). Gratings are fabricated in ethylene tetrafluoroethylene (ETFE) from nanopatterned silicon stamps using nanoimprinting. A sheet of ETFE (thickness 0.8 mm) is placed on a silicon stamp, heated to 200°C and placed under 30 Bar pressure for 300 s. The ETFE is cooled to 90°C while maintaining the same pressure, then released from the stamp. An optically opaque metal layer ( $\sim$ 120 nm thick Ti/Ag) is deposited onto the polymer to form metal gratings. Chemically synthesised CHPI powder [Sec. 2.3.2] is dissolved in tetrahydrofuran and spin coated onto the gratings in a dehydrated atmosphere to produce a conformal coating. For polystyrene (PS)-coated gratings,  $M_w = 500000$  PS powder is dissolved in toluene and spin coated onto the gratings. All samples are kept in a nitrogen purge dessication cabinet to prevent oxidation. Measurements by SEM and AFM of the metal and dielectric-coated gratings are used to

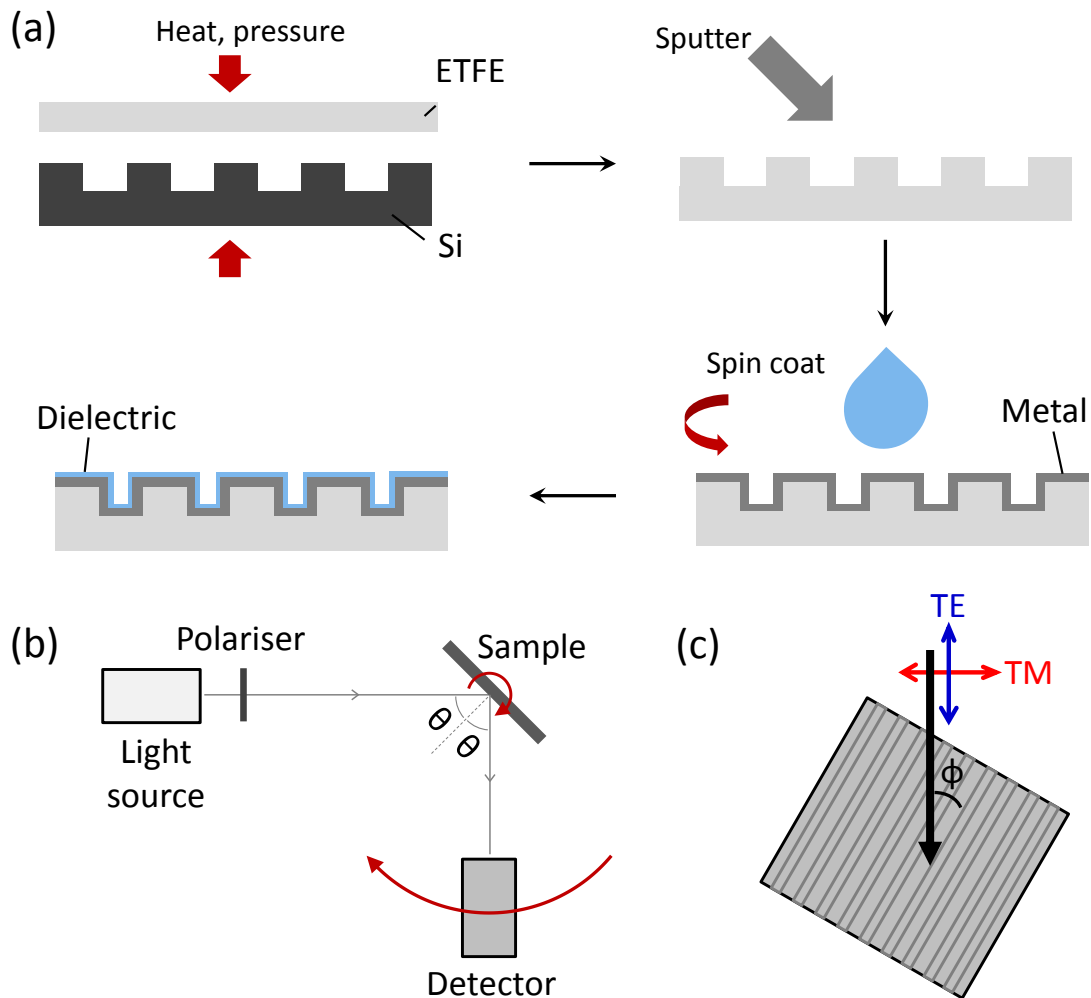


Fig. 7.1 (a) Fabrication of dielectric-coated metal grating. (b) Setup of angle-dependent reflectivity measurements. (c) Relationship between the polarisation of incoming light and azimuthal angle  $\phi$ . Red/blue arrows indicate the direction of the electric field.

extract the dimensions of the nanostructures. Polarised specular reflection measurements are made as a function of the incident polar ( $\theta$ ) and azimuthal ( $\phi$ ) angles using a polarised broadband white light source (215 – 2500 nm) [Figs. 7.1(b,c)]. The sample properties are uniform over  $\text{cm}^2$  areas, with small variations due to the depth and morphology of the coatings.

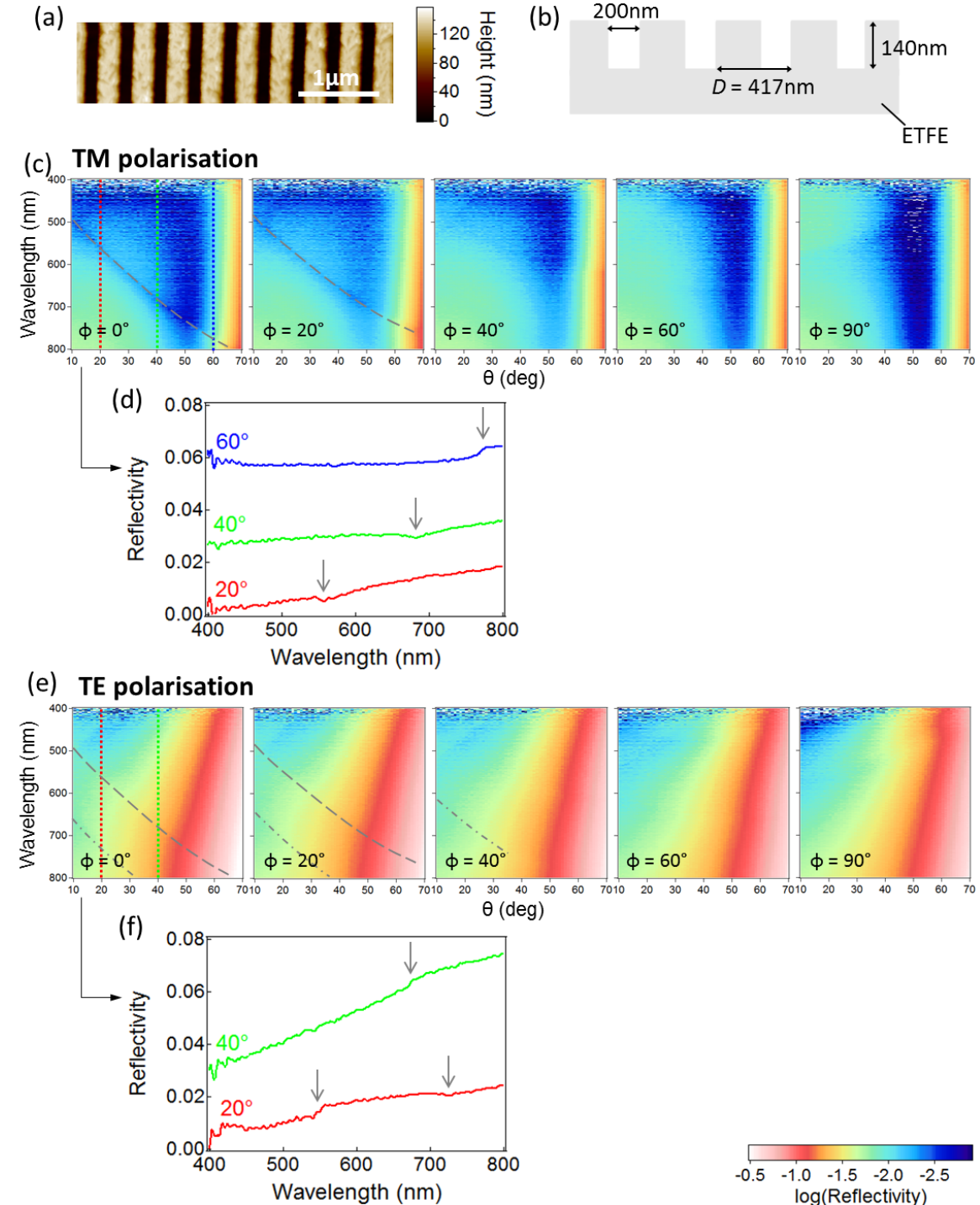


Fig. 7.2 (a) AFM image and (b) schematic structure of  $D = 417$  nm ETEFE grating. (c) TM polarised reflectivity scans of ETEFE grating, and (d) reflectivity spectra for  $\phi = 0^\circ$ . Spectra are offset for clarity. (e,f) Same as above for TE polarisation. Photonic grating modes are indicated by grey lines/arrows on reflectivity scans/spectra.

## 7.2 Dielectric gratings

### 7.2.1 ETFE gratings

AFM scans of the imprinted  $D = 417$  nm ETFE grating [Fig. 7.2(a)] show the formation of a square-wave grating with depth 140 nm and slit width 200 nm [Fig. 7.2(b)]. TM and TE polarised reflectivity scans show  $m = -1$  photonic modes in air according to Eq. 3.11 [grey dashed lines on Figs. 7.2(c,e)] appearing as dips in the reflectivity [Figs. 7.2(d,f)]. In TE polarisation we also see the appearance of a redshifted photonic mode (grey dot-dashed line on Fig. 7.2(e)), attributed to light that has penetrated the transmissive ETFE. This mode fits well to Eq. 3.11 with  $n = 1.4$ , the reported ETFE refractive index<sup>200</sup>. For both polarisations the grating modes are no longer visible for  $\phi > 60^\circ$ . Note also a dip in the reflectivity of TM scans at  $\theta \approx 50^\circ$  due to the Brewster angle of ETFE.

### 7.2.2 CHPI-coated ETFE gratings

The exciton resonance at 505 nm dominates both the TM and TE reflectivity scans of CHPI-coated  $D = 417$  nm ETFE gratings [Figs. 7.3(a,c)]. The  $m = \pm 1, n = 1.4$  diffractive photonic grating modes are again visible [grey dot-dashed lines on Figs. 7.3(a,c)], and appear as Fano resonances in reflectivity [Figs. 7.3(b,d)]. In TM polarisation the diffractive modes are strongest for  $\phi = 90^\circ$ , while for TE they are strongest at  $\phi = 0^\circ$ , thus coupling with photons is strongest when the  $\vec{E}$  field is parallel to grating lines. Note there are no interactions between grating modes and excitons in this system. The Brewster angle in TM scans has now changed to  $\theta \approx 62^\circ$  due to the larger refractive index of CHPI.

## 7.3 Non-plasmonic metal gratings

### 7.3.1 Ti gratings

SEM image of a  $D = 417$  nm Ti grating shows roughness in the sputtered Ti film on ETFE [Fig. 7.4(a)], while AFM measurements reveal a trapezoidal grating profile as a result of the nanoimprinting process. Heating and cooling of ETFE during sputtering also appears to have changed the grating periodicity  $D$ , as the photonic grating modes in reflectivity scans [Figs. 7.4(c,e)] are best fit to  $D = 410$  nm [Eq. 3.11]. Aside from the change in geometry, the appearance of  $m = -1$  grating modes in optical spectra is very similar to what was observed in ETFE gratings, with modes appearing as dips in reflectivity. However the coupling to

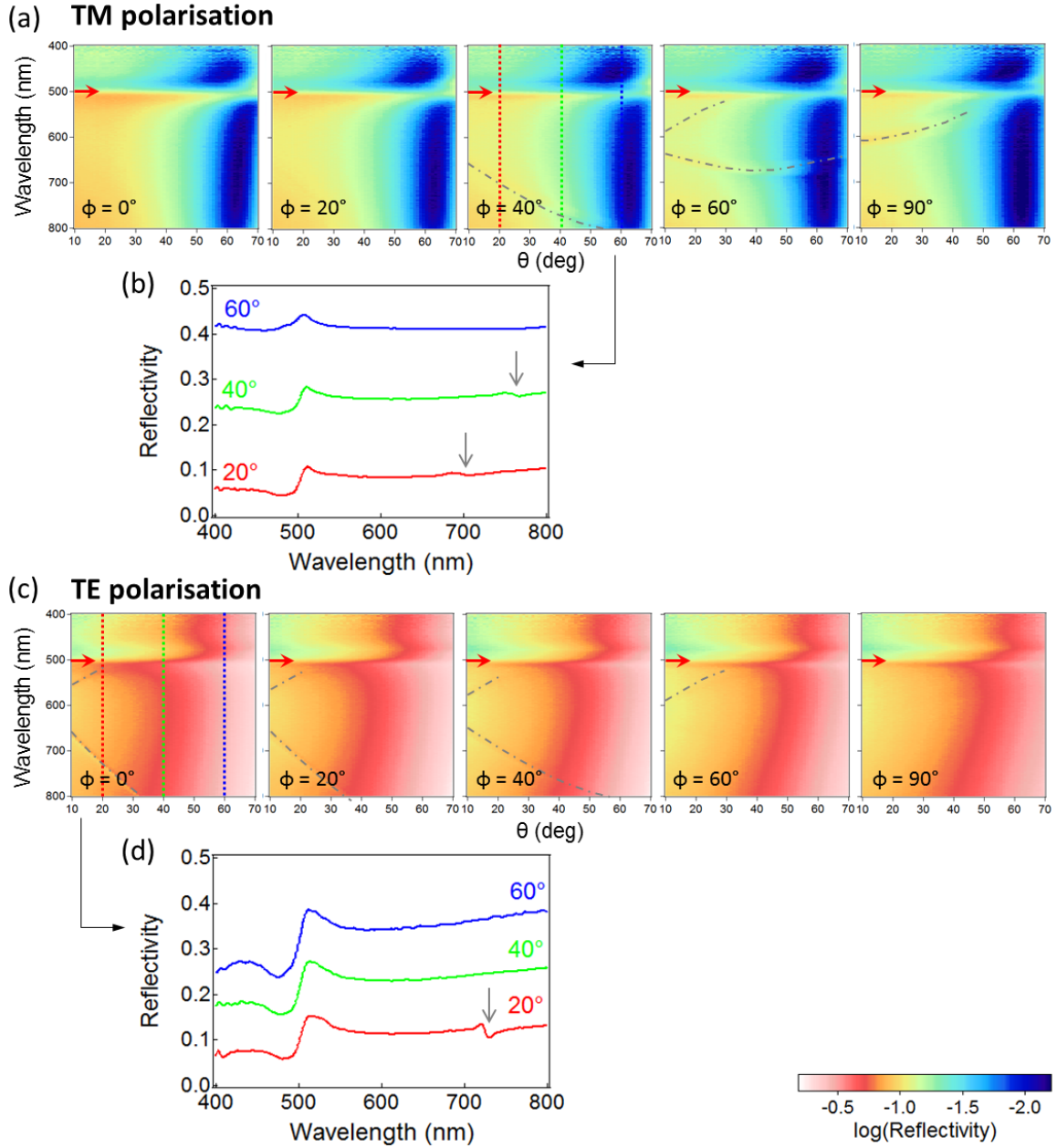


Fig. 7.3 (a) TM polarised reflectivity scans of  $D = 417$  nm CHPI-coated ETFE grating, and (b) reflectivity spectra for  $\phi = 40^\circ$ . Spectra are offset for clarity. (c) Same as (a) for TE polarisation and (d) reflectivity spectra for  $\phi = 0^\circ$ . Photonic grating modes are indicated by grey lines/arrows on reflectivity scans/spectra, and excitons by red arrows.

photons is much weaker in TE polarisation, as the  $\vec{E}$  field is parallel to grating lines [Sec. 3.2].

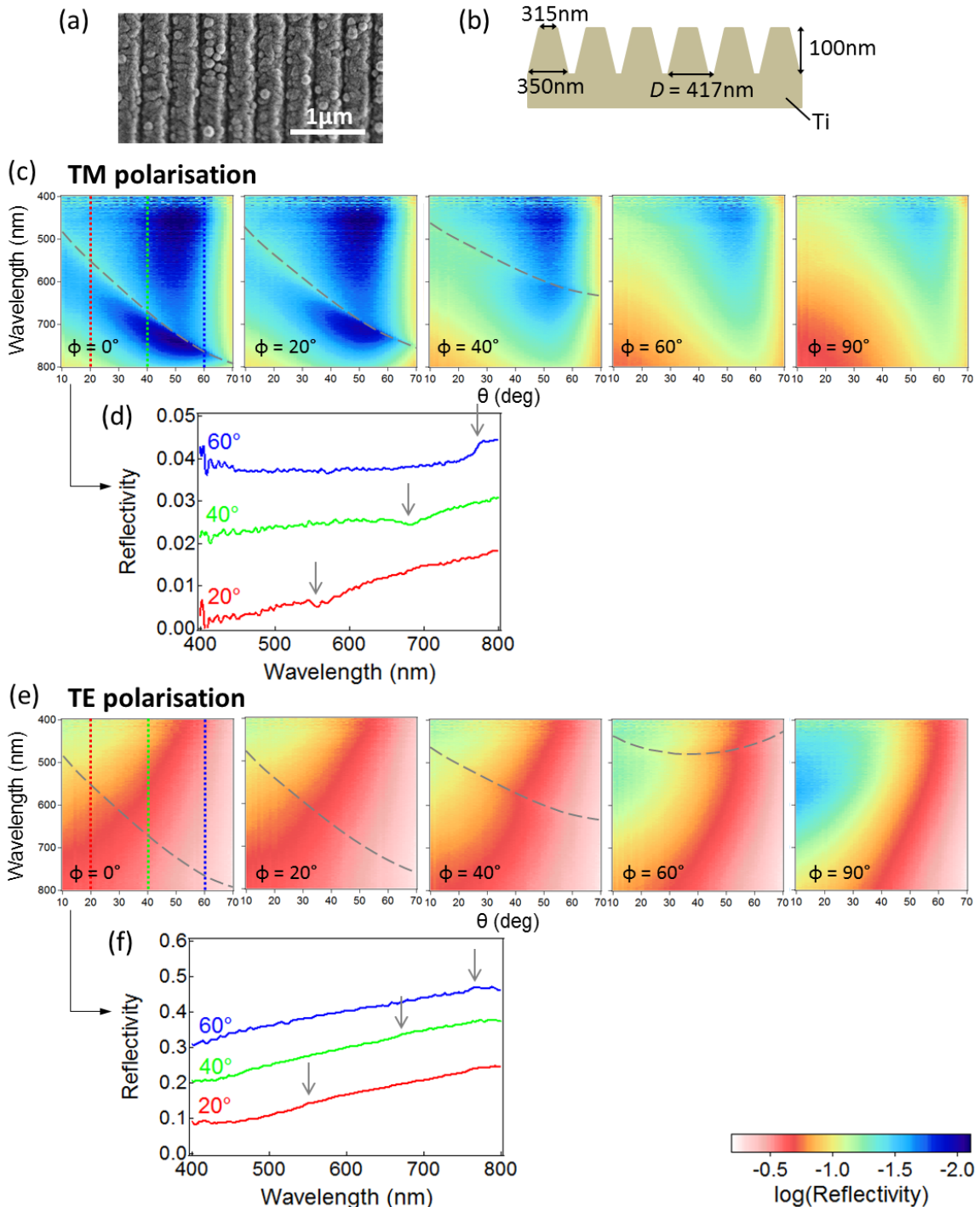


Fig. 7.4 (a) SEM image and (b) schematic structure of  $D = 417\text{ nm}$  Ti grating. (c) TM polarised reflectivity scans of Ti grating, and (d) reflectivity spectra for  $\phi = 0^\circ$ . Spectra are offset for clarity. (e,f) Same as above for TE polarisation. Photonic grating modes are indicated by grey lines/arrows on reflectivity scans/spectra.

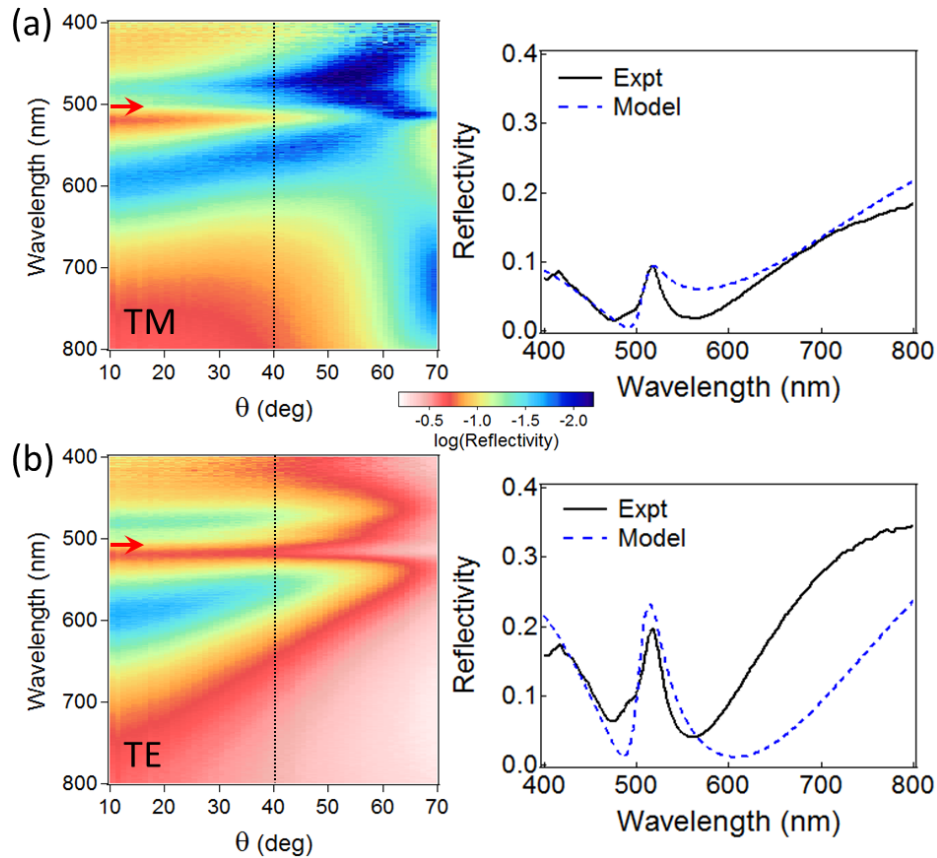


Fig. 7.5 Specular reflectivity scans of 70 nm CHPI film on 120 nm planar Ti film (left) with (a) TM and (b) TE polarised light. Excitons are marked by red arrows. Spectra at  $\theta = 40^\circ$  are plotted with those predicted by transfer matrix simulations (right).

### 7.3.2 CHPI-coated Ti gratings

Polarised reflectivity spectra of CHPI-coated planar Ti film [Fig. 7.5] show the appearance of an exciton resonance at 505 nm, indicating the excitons are unaffected by the metal film below. The experimental data fits well to transfer matrix simulations of 70 nm CHPI-coated 120 nm Ti film, and the differences observed can be attributed to non-uniformity and roughness in both the CHPI and Ti films.

AFM measurements show the metal grating is completely immersed in a non-uniform coating for  $D = 417$  nm CHPI-coated Ti grating [Figs. 7.6(a,b)]. As with CHPI-coated ETFE gratings, the exciton resonance at 505 nm dominates reflectivity spectra for both polarisations [Figs. 7.6(c,e)]. Although very weak dips can be seen to indicate diffractive  $m = -1$  grating modes in TM polarisation [Fig. 7.6(d)], coupling of TE-polarised light to grating modes is so weak that spectra appear almost identical to that of a CHPI-coated planar Ti film [Fig. 7.6(f)]. In both cases there are no interactions between CHPI excitons and modes of the Ti grating.

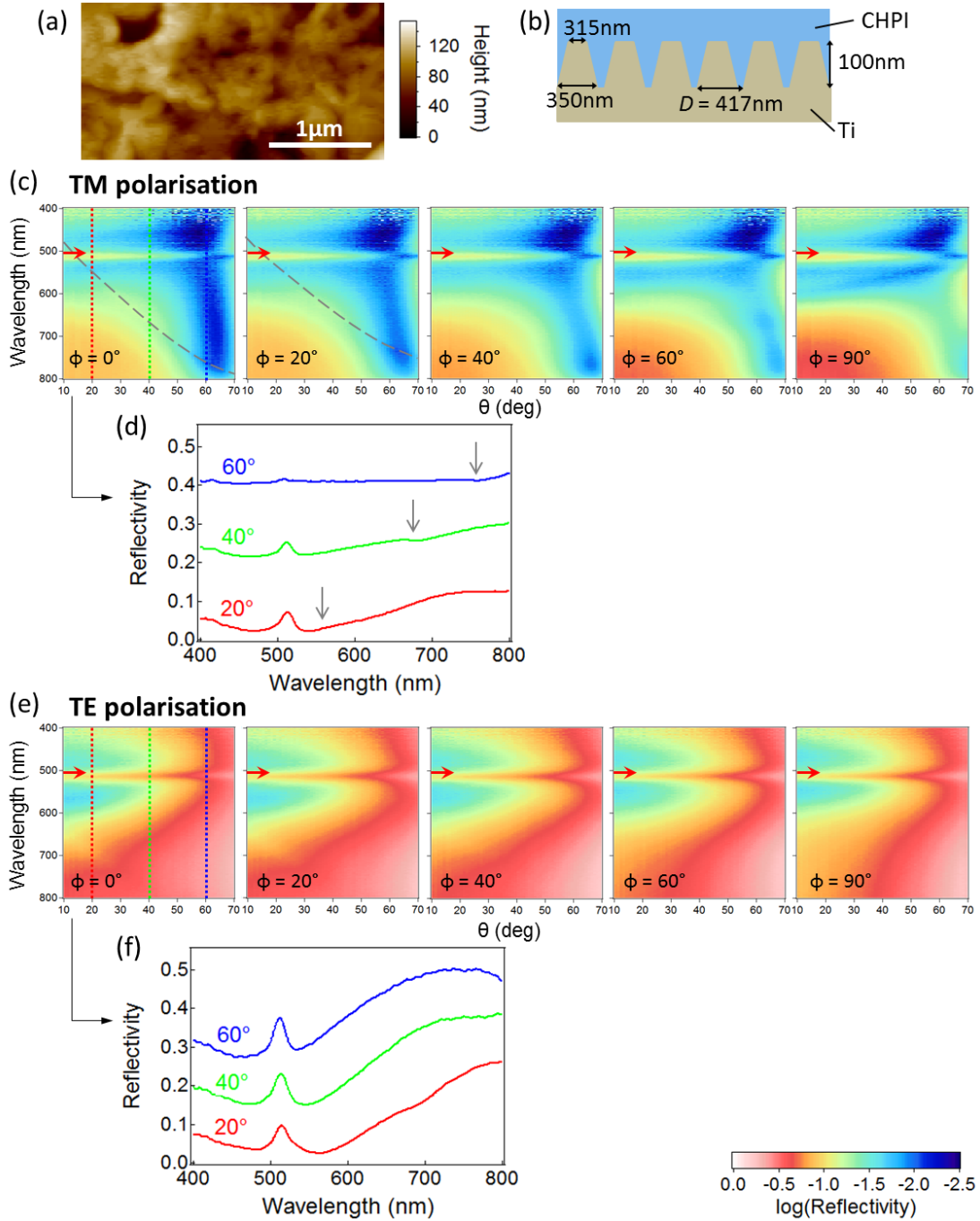


Fig. 7.6 (a) AFM image and (b) schematic structure of  $D = 417 \text{ nm}$  CHPI-coated Ti grating. (c) TM polarised reflectivity scans of  $D = 417 \text{ nm}$  CHPI-coated Ti grating, and (d) reflectivity spectra for  $\phi = 0^\circ$ . Spectra are offset for clarity. (e,f) Same as above for TE polarisation. Photonic grating modes are indicated by grey lines/arrows on reflectivity scans/spectra, and excitons by red arrows.

## 7.4 Plasmonic metal gratings

### 7.4.1 Ag gratings

Fig. 7.7 shows reflectivity scans for Ag gratings,  $D = 556, 417$  and  $278$  nm. The spectra for all three gratings show the same features: in TM polarisation a sharp threshold anomaly whose dispersion follows Eq. 3.11 for  $m = \pm 1$  (grey dashed lines), and a redshifted dip for the resonance anomaly indicating the presence of excited SPPs (black dashed lines). In TE polarisation we don't observe any anomaly features due to the inability to excite SPPs, instead we see the  $m = \pm 1$  photonic modes.

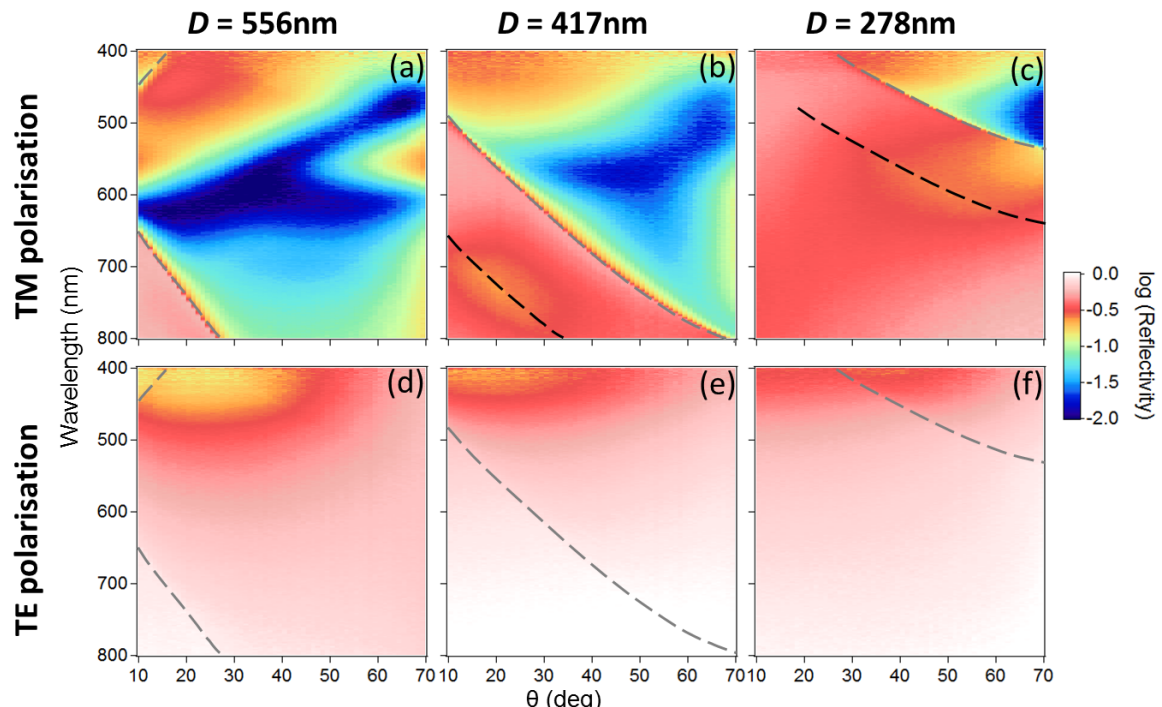


Fig. 7.7 Specular reflectivity scans of uncoated Ag gratings with periodicity  $D$  and polarisation of light as labelled. Photonic grating modes (threshold anomalies) are marked by grey dashed lines, and plasmonic grating modes (resonance anomalies) are marked by black dashed lines.

Focusing on the  $D = 417$  nm grating, we see that the sputtered Ag film on ETFE shows some roughness [Fig. 7.8(a)], and AFM measurements indicate a square-wave grating with depth 140 nm and slit width 130 nm [Fig. 7.8(b)]. In reflectivity the threshold anomalies (grey dashed lines) shift as expected according to Eq. 3.11 in TM polarisation [Fig. 7.8(c)], and appear as sharp changes in the intensity [Fig. 7.8(d)]. The redshifted resonance anomalies (black dashed lines) become weaker with increasing  $\phi$  and are no longer observed when

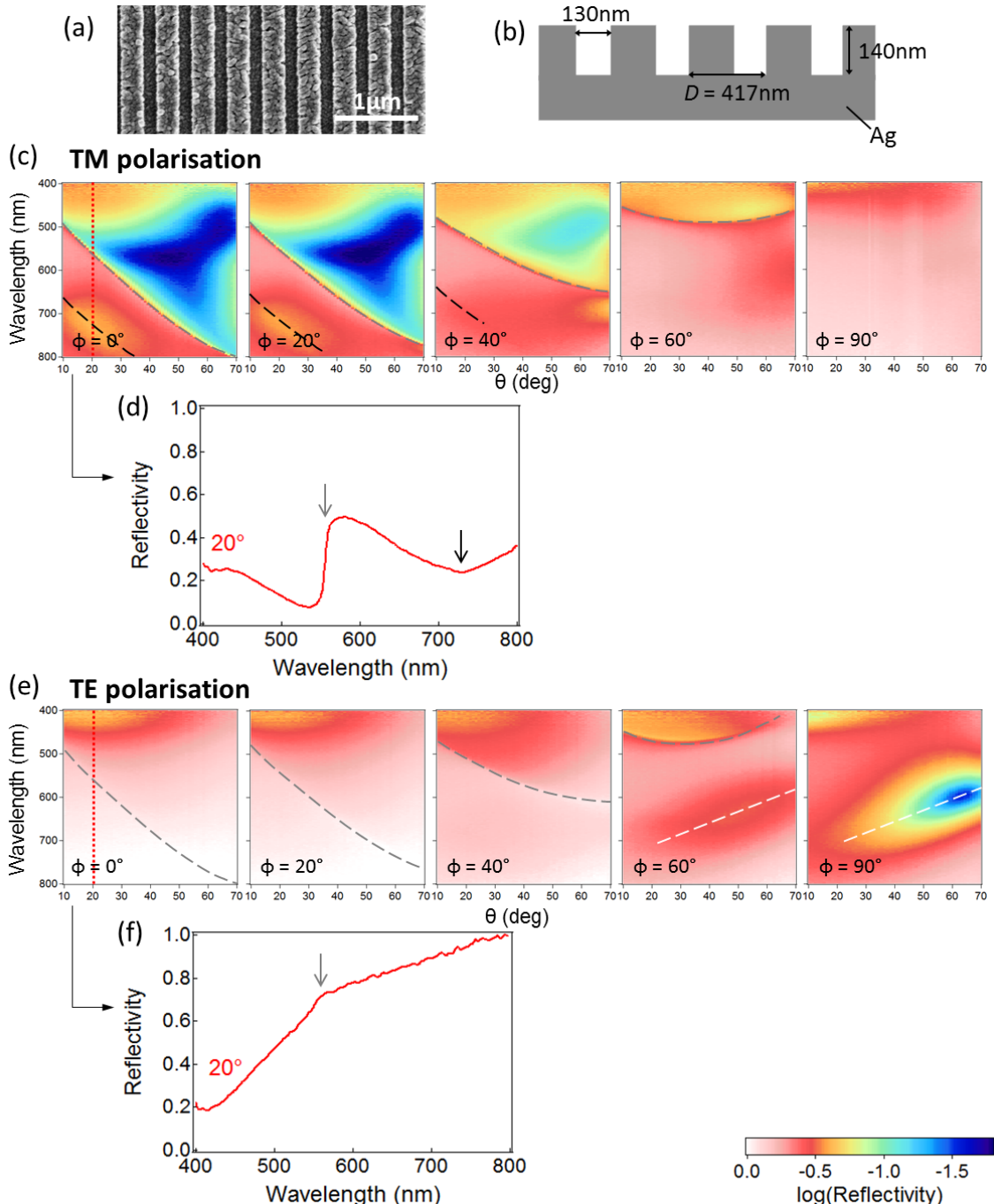


Fig. 7.8 (a) SEM image and (b) schematic structure of  $D = 417\text{ nm}$  Ag grating. (c) TM polarised reflectivity scans of  $D = 417\text{ nm}$  Ag grating, and (d) reflectivity spectra for  $\phi = 0^\circ$ . (e,f) Same as above for TE polarisation. Photonic grating modes (threshold anomalies) are indicated by grey lines/arrows on reflectivity scans/spectra, plasmonic gratings modes (resonance anomalies) by black lines/arrows, and Fabry-Perot modes by white dashed lines (see text).

$\phi > 60^\circ$  as it becomes harder for photons to couple to SPPs. For the same reason no anomalies are observed in TE polarisation at low  $\phi$ , where the photonic modes appear weakly in spectra [Fig. 7.8(f)]. We would expect to observe anomalies at  $\phi = 90^\circ$  in TE polarisation, however the energy of the mode is too high for our measurement range here. The broad dip seen at  $\phi = 60^\circ$ – $90^\circ$  in TE polarisation (white dashed lines) is assigned to the Fabry-Perot interference mode of light reflected from the top and bottom surfaces of the grating. This mode doesn't change in position with  $\phi$  and extrapolates to  $\sim 750$  nm at  $\theta = 0^\circ$ , which fits the height of the gratings as seen in AFM measurements.

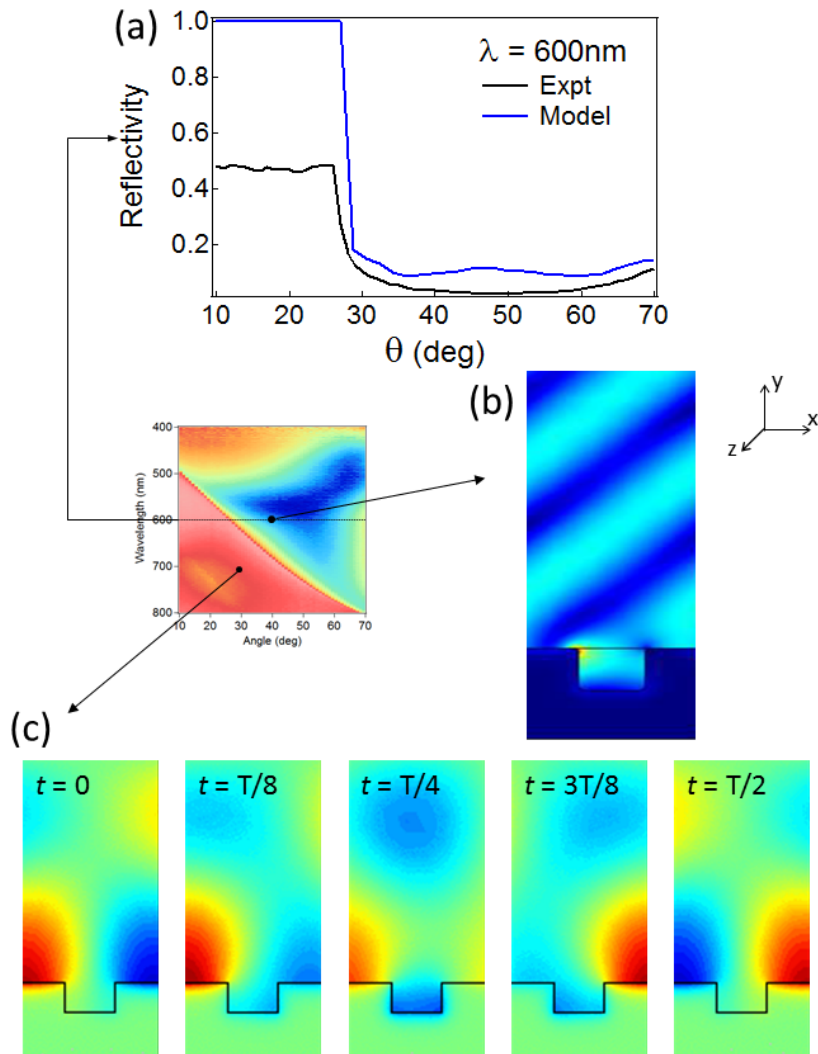


Fig. 7.9 (a) Experimental and modelled TM reflectivity spectra of  $D = 417$  nm Ag grating for  $\phi = 0^\circ$   $\lambda = 600$  nm. (b) Time averaged  $\vec{E}$  field intensity ( $\vec{E} \cdot \vec{E}$ ) profile for  $\lambda = 600$  nm  $\theta = 40^\circ$ . (c)  $H_z$  nearfield profile at time  $t$  of the optical cycle  $T$  for  $\lambda = 700$  nm  $\theta = 30^\circ$ .

We use finite element method (FEM) to model the electromagnetic nearfield of grating modes in order to understand their behaviour. The modelled spectrum for  $\phi = 0^\circ \lambda = 600 \text{ nm}$  agrees very well with features of the experimental data [Fig. 7.9(a)], but has a larger reflectivity overall as the model does not take into account the Ag film roughness. Low efficiency of the specularly reflected grating order gives rise to the low reflection region seen at high  $\theta$ , instead the coupling is strongest to the  $-1$  diffracted order as shown in Fig. 7.9(b). The modelled  $H_z$  field component of the resonance anomaly shows that it does indeed behave like SPP travelling on the surface of the metal [Fig. 7.9(c)].

The position of the threshold anomaly is fixed by the periodicity of the structure, however as the resonance anomaly is caused by the interference between diffracted light and SPPs we expect its position to be much more sensitive to the geometry of the grating. Fig. 7.10 shows the profiles and TM reflectivity scans at  $\phi = 0^\circ$  of three different gratings, ranging from square-wave [Fig. 7.10(a)] to approximately sinusoidal [Fig. 7.10(b,c)]. The sharp threshold anomalies (grey dashed lines) remain in the same position for all three gratings, barring small changes in  $D$  as a result of the sputtering process. However the widths and positions of the resonance anomalies vary greatly with geometry, and the sharpest resonances are produced by sinusoidal gratings. We also observe a dispersionless mode at  $\sim 450 \text{ nm}$  in Figs. 7.10(b,c) that may be due to the presence of channel plasmons, which require a narrowing of the grating slit as seen in the sinusoidal gratings.

#### 7.4.2 PS-coated Ag gratings

From the AFM image of  $D = 417 \text{ nm}$  PS-coated grating [Fig. 7.11(a)] we see that the Ag grating is almost submerged beneath the non-uniform PS layer, resulting in a shallow sinusoidal grating with an average height of 5 nm [Fig. 7.11(b)]. The presence of the PS overcoating increases the complexity of the reflectivity spectra by allowing access to more modes. In both TM and TE polarisation, photonic (grey dashed lines) and redshifted plasmonic modes (black dashed lines) can be observed [Fig. 7.11(c,e)], however the photonic mode is much weaker in TE polarisation. At high  $\phi$  in TM polarisation, a second set of plasmonic modes can be seen (black dot-dashed lines), likely due to the differing PS thickness at the top and bottom surface of the grating. We also see a broader mode at  $\sim 560 \text{ nm}$  for  $\phi = 0^\circ \theta = 10^\circ$  in both polarisations, which remains in roughly the same position for all  $\phi$  (purple dashed line).

Using FEM, we observe two types of modes at  $\phi = 90^\circ$  in TM polarisation. A mode at higher energy has field intensity concentrated at the top surface of the grating, and

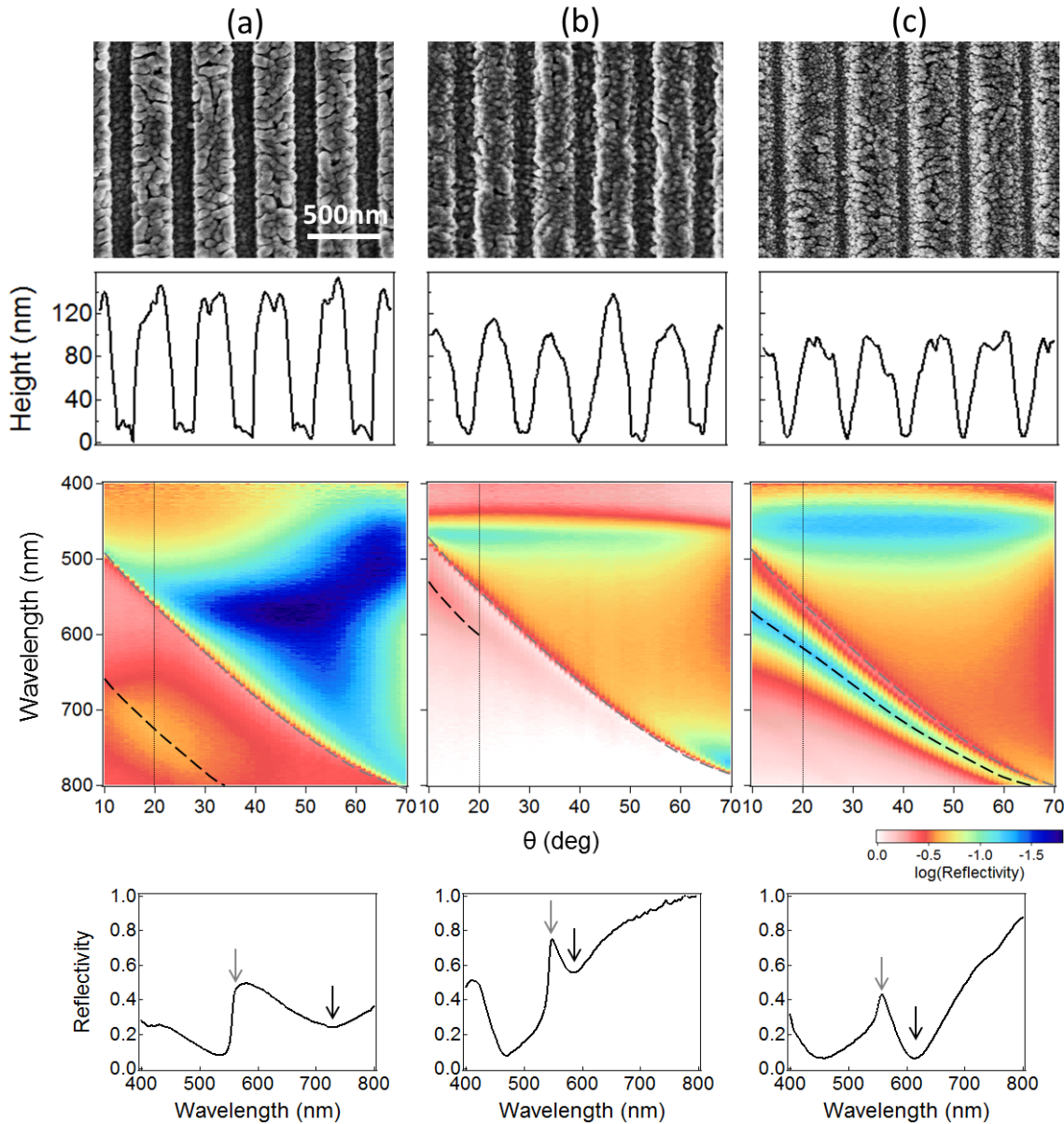


Fig. 7.10 (From top) SEM image, AFM profile, TM specular reflectivity scans at  $\phi = 0^\circ$ , and reflectivity spectra at  $\phi = 0^\circ \theta = 20^\circ$  for three  $D = 417 \text{ nm}$  Ag gratings. Photonic grating modes (threshold anomalies) are marked by grey dashed lines/arrows, and plasmonic grating modes (resonance anomalies) by black dashed lines/arrows on reflectivity scans/spectra.

evanescently decays from the Ag surface [Fig. 7.12(a)]. Taking snapshots throughout the optical cycle, the mode appears to be a quasiparticle travelling along the top surface of the grating [Fig. 7.12(b)]. By varying the geometry of the grating, we find the mode decreases in energy as  $D$  increases, increases in energy with the slit width, and is unaffected by grating height, thus showing the behaviour expected for an SPP mode. On the other hand, the

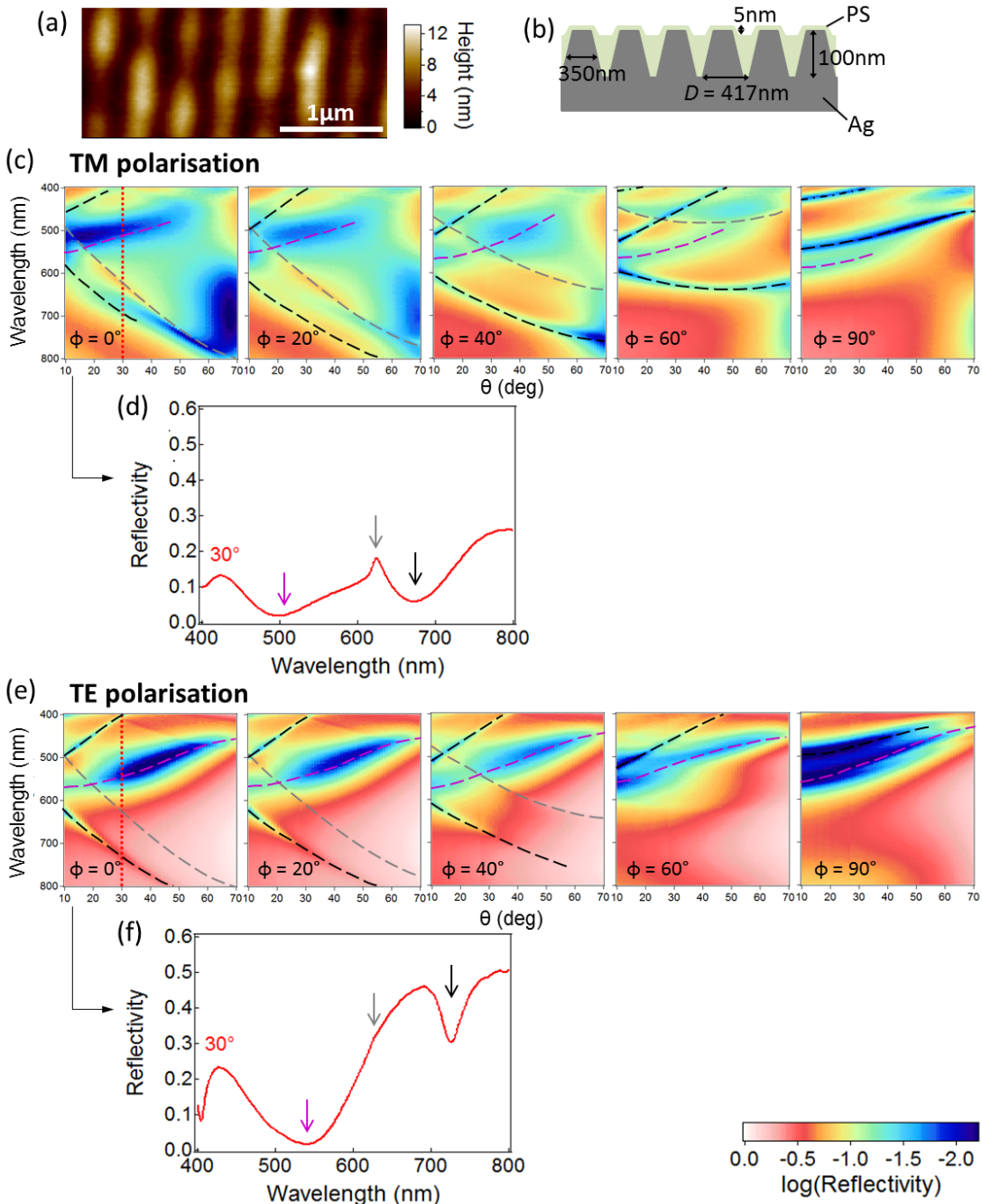


Fig. 7.11 (a) AFM image and (b) schematic structure of  $D = 417 \text{ nm}$  PS-coated Ag grating. (c) TM polarised reflectivity scans of PS-coated Ag grating, and (d) reflectivity spectra for  $\phi = 40^\circ$ . (e) Same as above for TE polarisation, and (f) reflectivity spectra for  $\phi = 0^\circ$ . Photonic grating modes are indicated by grey lines/arrows on reflectivity scans/spectra, plasmonic gratings modes by black lines/arrows, and waveguide modes by purple lines/arrows.

field intensity of the lower energy mode is mainly concentrated in the slit of the grating [Fig. 7.12(c)], and appears to travel along the slit [Fig. 7.12(d)]. The energy of the mode is unaffected by  $D$  or the grating height, and decreases as the slit width increases, the behaviour of a mode waveguided by the grating slit. According to Eq. 3.13 the dispersion fits that of a TE<sub>10</sub> mode.

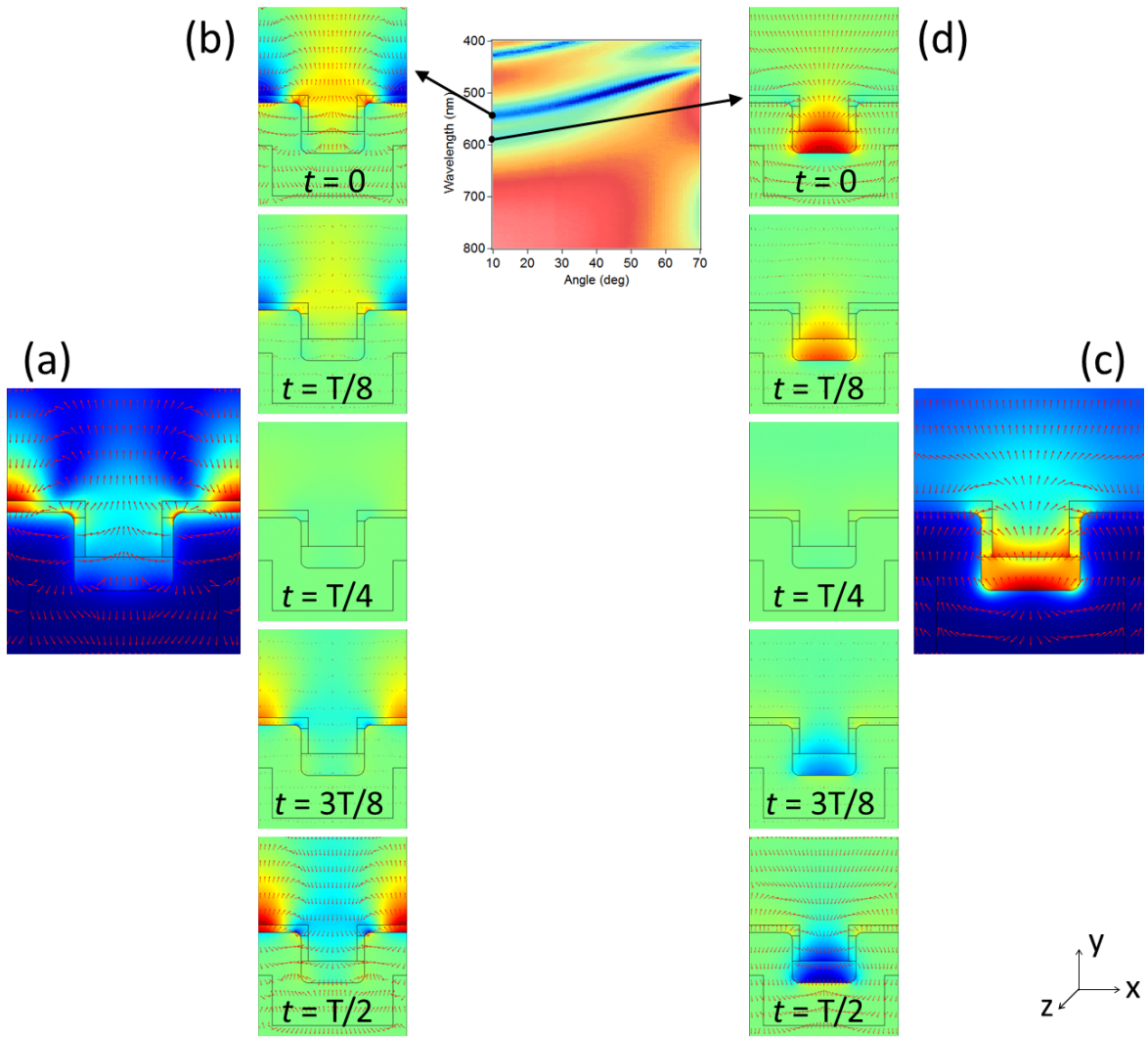


Fig. 7.12 (a) Time averaged and (b) snapshots at time  $t$  in the optical cycle  $T$  of the  $E_y$  nearfield intensity for the higher energy (plasmonic) mode at  $\phi = 90^\circ \theta = 10^\circ$ . (c,d) Same as above for the lower energy (waveguide) mode. Arrows represent the size and direction of the  $\vec{E}$  field vector.

Both SPP and waveguided modes are very sensitive to the dielectric environment as shown by Eqs. 3.11 and 3.13, and Fig. 7.13 shows the change in these modes with increasing PS thickness. Both the narrower SPP resonances (black dashed lines) and broader waveguided

modes (purple dashed lines) redshift with increasing PS coverage as expected. For the structure in Fig. 7.13(c) these two modes actually overlap, although no interactions occur.

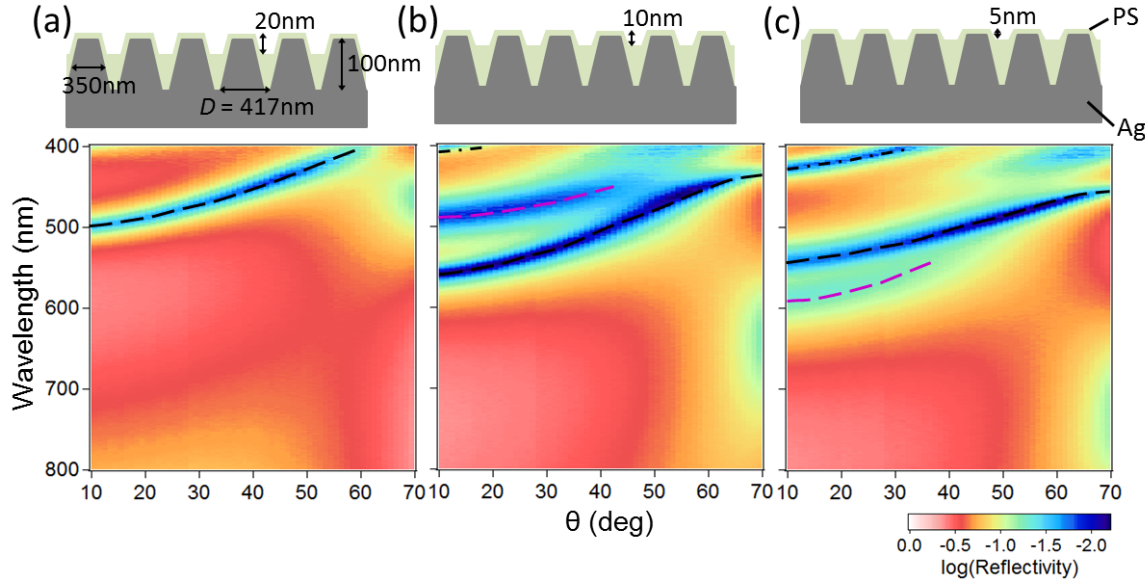


Fig. 7.13 Schematic structure of PS-coated  $D = 417$  nm Ag gratings (top), and TM polarised reflectivity scans at  $\phi = 90^\circ$  (bottom). PS thickness increases from (a) → (c). Plasmonic modes are indicated by black lines, and waveguide modes by purple lines.

### 7.4.3 CHPI-coated Ag gratings

Fig. 7.14 shows TM reflectivity scans for CHPI-coated Ag gratings,  $D = 556$ , 417 and 278 nm at  $\phi = 0$  and  $90^\circ$ . The spectra for  $D = 556$  and 417 nm are very similar, showing two exciton modes (red arrows) that strongly couple to an SPP grating mode (black dashed line) as the oscillations become resonant at  $\phi = 90^\circ$ . Two excitons can also be observed for  $D = 278$  nm, however the SPP mode is at a higher energy and thus the coupling occurs at  $\phi = 0^\circ$ .

TM polarised reflectivity scans of  $D = 417$  nm CHPI-coated Ag grating at  $\phi = 0^\circ$  [Fig. 7.15(a)] show two dispersionless exciton modes at 480 and 500 nm (marked by arrows) far off resonance with grating modes. The persistent presence of a second exciton is only detected when SPPs can be excited, i. e. in TM polarisation [Fig. 7.15(a)] but not TE [Fig. 7.15(b)], nor in CHPI-coated planar Ag films [Fig. 7.15(c)]. It is also not observed for CHPI-coated non-plasmonic gratings [Figs. 7.3 and 7.6], thus from Fig. 7.15 we deduce that SPP excitation leads to the observation of an additional redshifted exciton with a splitting of 100 meV. Its appearance only when SPPs are present rules out any influence from modified CHPI assembly in the grooves, which are in any case hundreds of times larger than the PbI

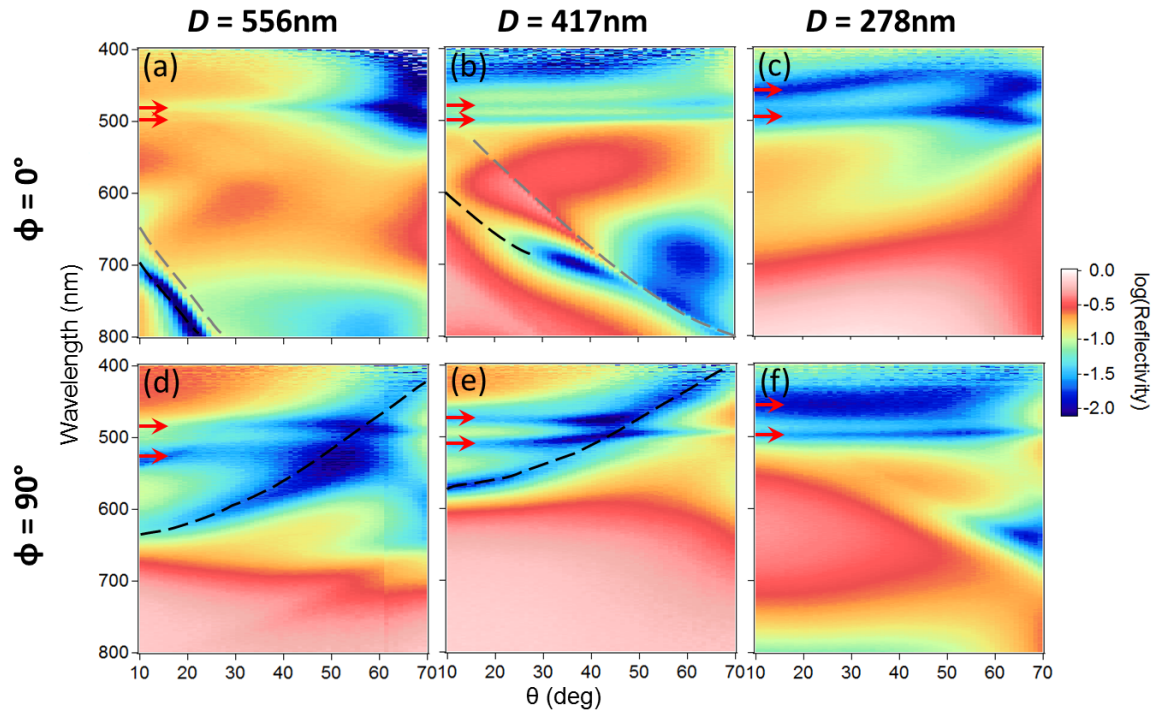


Fig. 7.14 TM specular reflectivity scans of CHPI-coated Ag gratings with  $D$  and  $\phi$  as labelled. Photonic grating modes are marked by grey dashed lines, plasmonic grating modes by black dashed lines, and excitons indicated by red arrows.

layer spacing. In addition the exciton diffusion length in 2D perovskites is of order  $10\text{ nm}^{92}$ , therefore we do not expect any limiting effects due to the grating geometry. We note slight changes in the CHPI coverage alter the positions and intensities of dispersive grating modes [*cf* Fig. 7.17(c), with a thinner CHPI coating], however the exciton modes remain essentially unchanged.

It is well known that the emitted energy of a dipole (exciton) is lowered when placed in front of a metallic surface due to interactions between the dipole and the reflected electromagnetic field<sup>201–206</sup>. Using the method of images, we can replace the metal and describe instead the coupling between an exciton in the CHPI ( $\epsilon_1$ ) and its image exciton in the metal ( $\epsilon_2$ ), modified by their respective dielectric environments. Chance *et al.*<sup>204</sup> showed the redshift in the emitted energy of an exciton ( $\Delta E_{ex}$ ) oriented parallel to the interface can be approximated by

$$\Delta E_{ex} \sim \left( \frac{1}{k_1 l} \right)^3 \operatorname{Re} \left\{ \frac{\epsilon_2 - \epsilon_1}{\epsilon_2 + \epsilon_1} \right\} \Gamma_0, \quad (7.1)$$

where  $l$  is the distance between the exciton and a metal surface,  $k_1$  is the wavenumber of light in CHPI,  $q$  is the quantum yield of CHPI excitons (taken here to be 1), and  $\Gamma_0$  is the

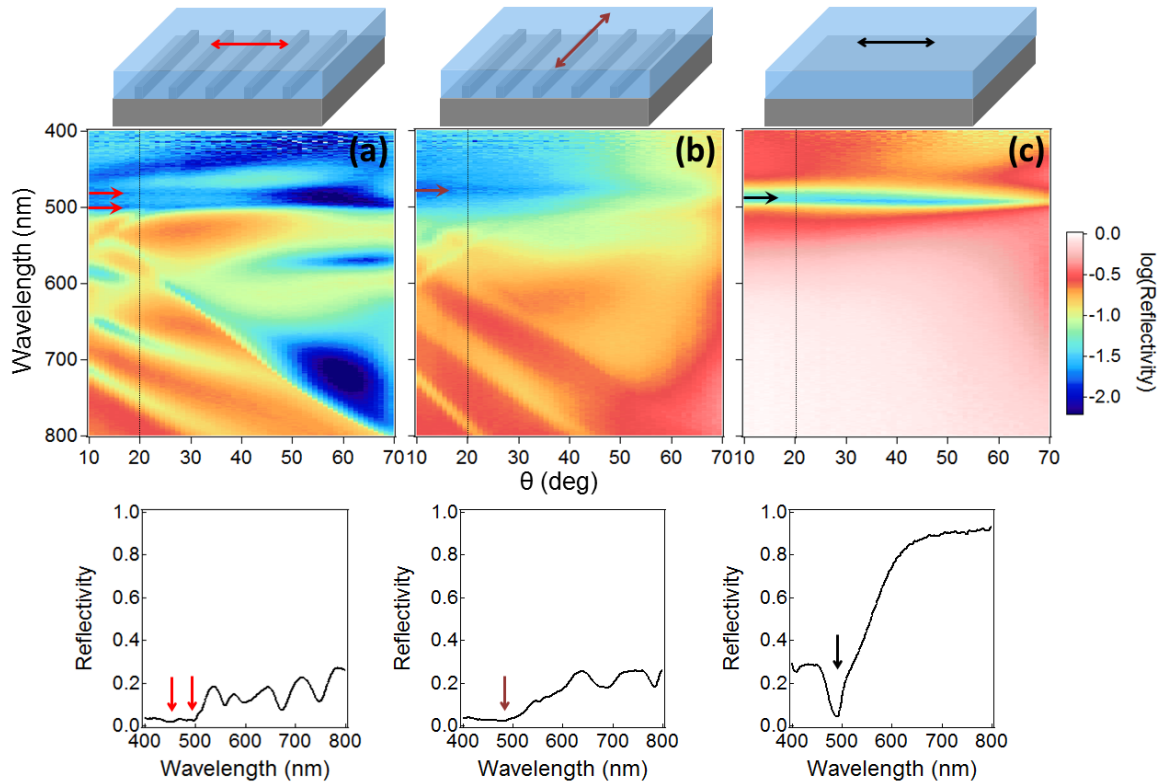


Fig. 7.15 Specular reflectivity scans at  $\phi = 0^\circ$ : CHPI-coated Ag grating with (a) TM and (b) TE polarised light, and (c) CHPI-coated 120 nm planar Ag film with TM polarised light. The electric field orientation is shown above each scan, the reflectivity spectra at  $\theta = 20^\circ$  below, and positions of exciton modes are indicated by arrows.

inverse exciton radiative lifetime without the metal. Similar to the appearance of excitons in the spectra, we expect to observe such coupled ‘image-biexcitons’ as minima in the reflectivity, at a wavelength that differs from the uncoupled exciton according to Eq. 7.1. The strength of coupling between the exciton and reflected electromagnetic field depends on the exciton dipole moment, which is controlled by the term  $q\Gamma_0$ . From this we can see the  $l^{-3}$  dependence of the redshift as shown in Fig. 7.16(a), where the experimentally observed  $\Delta E_{ex} \sim 100$  meV corresponds to  $l \sim 22$  nm, close to the experimentally-determined CHPI thickness. Clearly  $\Delta E_{ex}$  is also affected by the dielectric response of CHPI and Ag, and from Eq. 7.1 we see that  $\Delta E_{ex}$  is maximised if  $\epsilon_2 + \epsilon_1 \rightarrow 0$ , i. e. when emission is resonant with an SPP on the metal-dielectric interface. The linewidth of the exciton is also affected by interactions with image charges in the metal, however in our perovskite system this effect is not dominant due to tight planar confinement of excitons. We expect larger effects in systems that are less perfectly 2D, such as semiconductor heterostructures and J-aggregate systems, where surface charges play a much larger role.

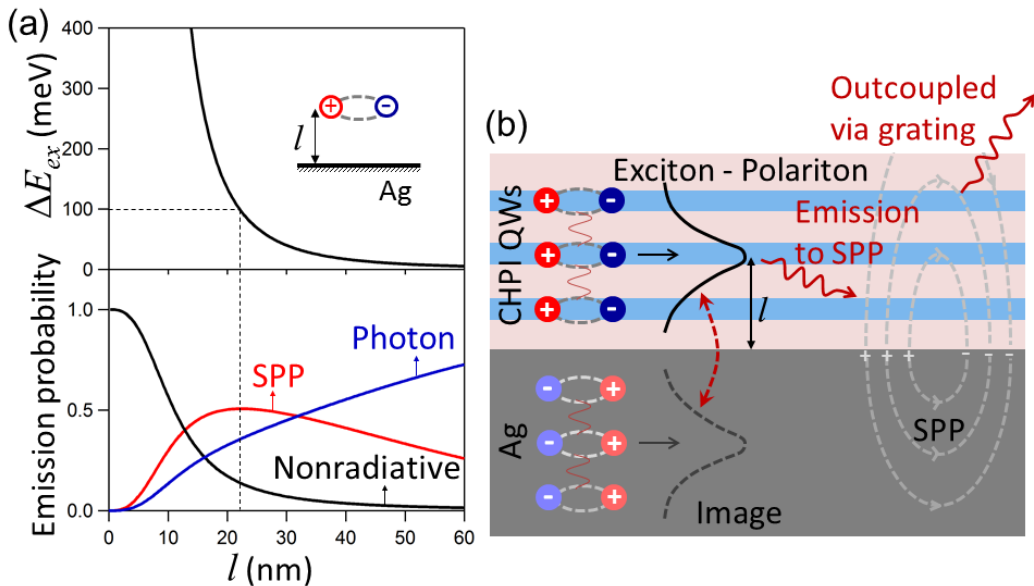


Fig. 7.16 (a) Change in emitted energy (top) and relative decay probabilities (bottom) of an exciton with energy 2.6 eV placed distance  $l$  from the Ag surface. The dashed line indicates the experimentally measured redshift. (b) Schematic mechanism for SPP-mediated emission of image-biexciton.

The role of the SPP in this case is to outcouple the signal of the redshifted exciton. There are three main decay channels for dipole emission near a metal surface: direct emission to photons, emission to SPPs, and nonradiative processes such as the excitation of electron-hole pairs and lossy surface waves on the metal. Other nonradiative paths via defects or phonons are independent of  $l$  and will be ignored in this analysis. Emission into SPPs provides an extra radiative decay channel as this signal can be extracted to the far field via the periodic nanostructure, and this mechanism has been used to improve the luminescence efficiency of light emitting devices<sup>207,208</sup>. The relative decay probability for each process is calculated as a function of  $l$ <sup>206</sup> and shown in Fig. 7.16(a). Although these calculations are intended for SPPs propagating on planar metal surfaces, we can use them as approximations for our grating system, although we note such estimates are indeed expected to become less accurate with increasing structure depth. Up to a CHPI thickness of 25 nm, SPP mediated emission is the most important radiative decay channel with a maximum emission probability at 22 nm, matching the experimentally observed  $\Delta E_{ex}$ . Even for thicker CHPI films we expect the exciton modes to remain at the same positions, because SPP emission becomes weak at large  $l$  where  $\Delta E_{ex}$  is negligible.

In our MQW perovskite system, localised excitons in periodically-spaced nearby QWs are optically coupled together to form collective exciton-polariton states an average distance

$l$  from the Ag surface<sup>209–212</sup>. Therefore in CHPI-coated Ag gratings we observe both in-plane exciton-polaritons, and out-of-plane interactions that lead to ‘image-biexcitons’, which are outcoupled via SPP emission with a binding energy of 100 meV at room temperature [Fig. 7.16(b)]. For our grating system, the exciton and SPP modes become closer in energy with increasing  $\phi$  [see below and Fig. 7.17(c)], and as a result splitting between the exciton modes (indicated by arrows in Fig. 7.17(c)) increases to around 185 meV at  $\phi = 90^\circ$ . The azimuthal dependence of the exciton splitting reflects the tuneable modification of the Coulomb interaction in this geometry, but however requires further theoretical development.

AFM image of a  $D = 417$  nm CHPI-coated Ag grating shows a clear grating structure despite the roughness of CHPI coating [Fig. 7.17(a)]. Using AFM measurements, we find CHPI forms a conformal coating around the Ag grating with thickness  $\sim 25$  nm [Fig. 7.17(c)]. In TE polarisation, we only observe the presence of one exciton without the signature of any grating modes, similar to the CHPI-coated Ti gratings. In TM polarised reflectivity scans, as well as strong excitons (red arrows) we also observe  $m = \pm 1$  photonic and plasmonic grating modes [Fig. 7.17(c)]. As the SPP modes become resonant with the exciton and image exciton, the light-matter modes strongly couple and produce an anticrossing in the reflectivity of 0.25 eV. Extracting the mode positions from the  $\phi = 90^\circ$  scan [Fig. 7.17(c)] allows them to be fit to a three oscillator model using the Hamiltonian

$$\hat{H} = \begin{pmatrix} E_{ex} & 0 & \Omega_{ex}/2 \\ 0 & E_{bx} & \Omega_{bx}/2 \\ \Omega_{ex}/2 & \Omega_{bx}/2 & E_{pl} \end{pmatrix}, \quad (7.2)$$

where  $E_{ex}$ ,  $E_{bx}$  and  $E_{pl}$  are the energies of the exciton-polariton, image-biexciton and plasmonic grating modes respectively, while  $\Omega_{ex}$  and  $\Omega_{bx}$  represent the interaction between the SPP and exciton/image-biexciton. From this we find Rabi splittings of  $\Omega_{ex} = 150$  meV and  $\Omega_{bx} = 125$  meV. These are greatly enhanced because of the large confinement of the plasmonic optical field in the thin PbI QW layers. The Rabi splitting is given by  $\Omega \propto \sqrt{f_{osc}N_{QW}/V}$ , where the oscillator strength ( $f_{osc}$ ) of the CHPI is assumed to be similar for coupling to photons or plasmons, the number of QWs ( $N_{QW}$ ) is proportional to the CHPI thickness, and the mode volume ( $V$ ) is here proportional to the optical mode size. Comparing to Fabry-Perot planar CHPI microcavities in strong coupling<sup>43</sup> which have CHPI thickness of 72 nm, cavity length of 407 nm, and a Rabi frequency of  $\Omega_{FP} = 65$  meV, the simple scaling above predicts  $\Omega_{SPP} \sim \Omega_{FP} \sqrt{(22/72).(407/22)} = 156$  meV, in excellent agreement with our measurements. Using SPPs to strongly couple to the excitons thus dramatically reduces the cavity length, thus enhancing the light-matter coupling.

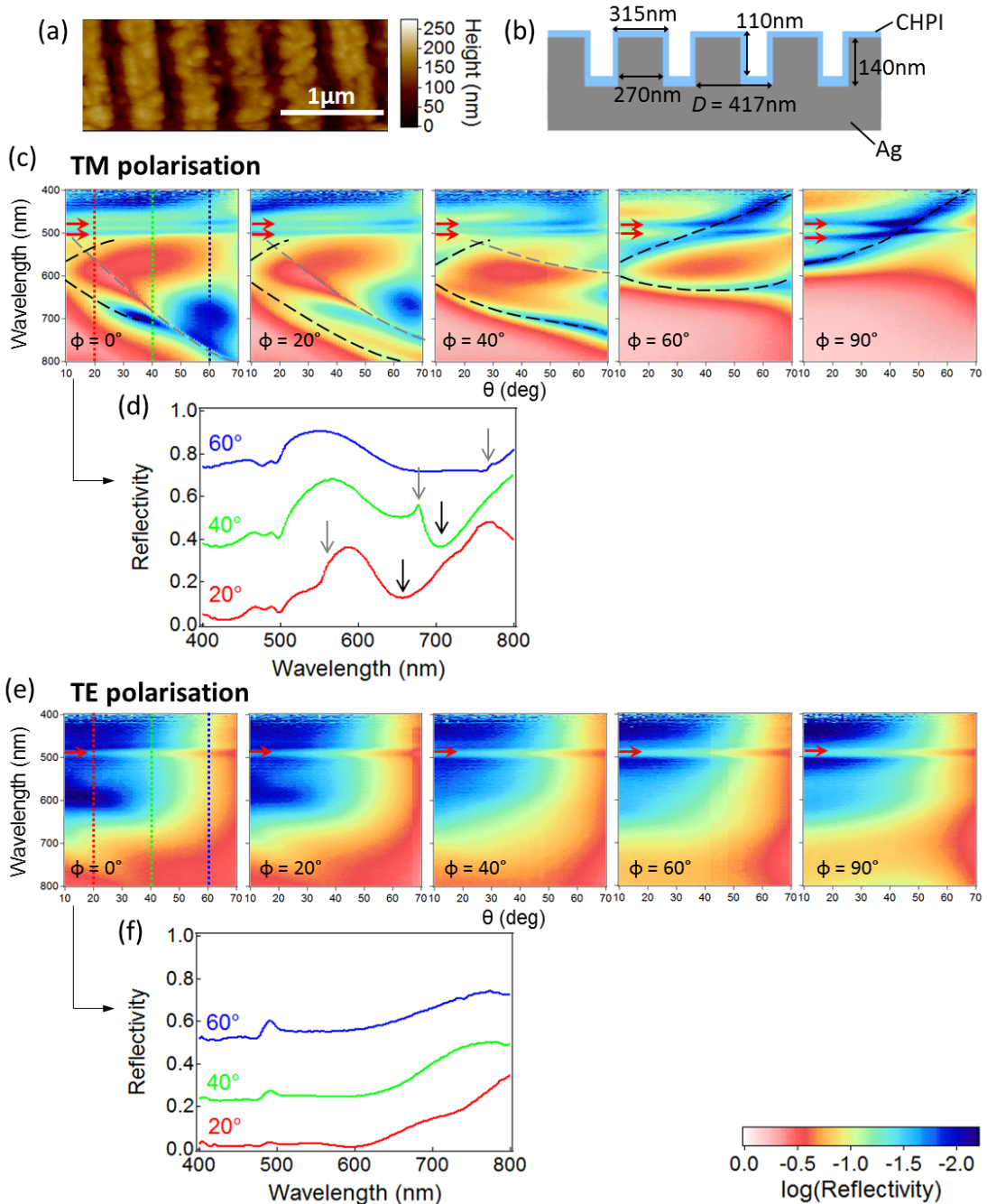


Fig. 7.17 (a) AFM image and (b) schematic structure of  $D = 417$  nm CHPI-coated Ag grating. (c) TM polarised reflectivity scans of  $D = 417$  nm Ag grating, and (d) reflectivity spectra for  $\phi = 0^\circ$ . Spectra are offset for clarity. (e,f) Same as above for TE polarisation. Photonic grating modes are indicated by grey lines/arrows on reflectivity scans/spectra, plasmonic gratings modes by black lines/arrows, and excitons by red arrows.

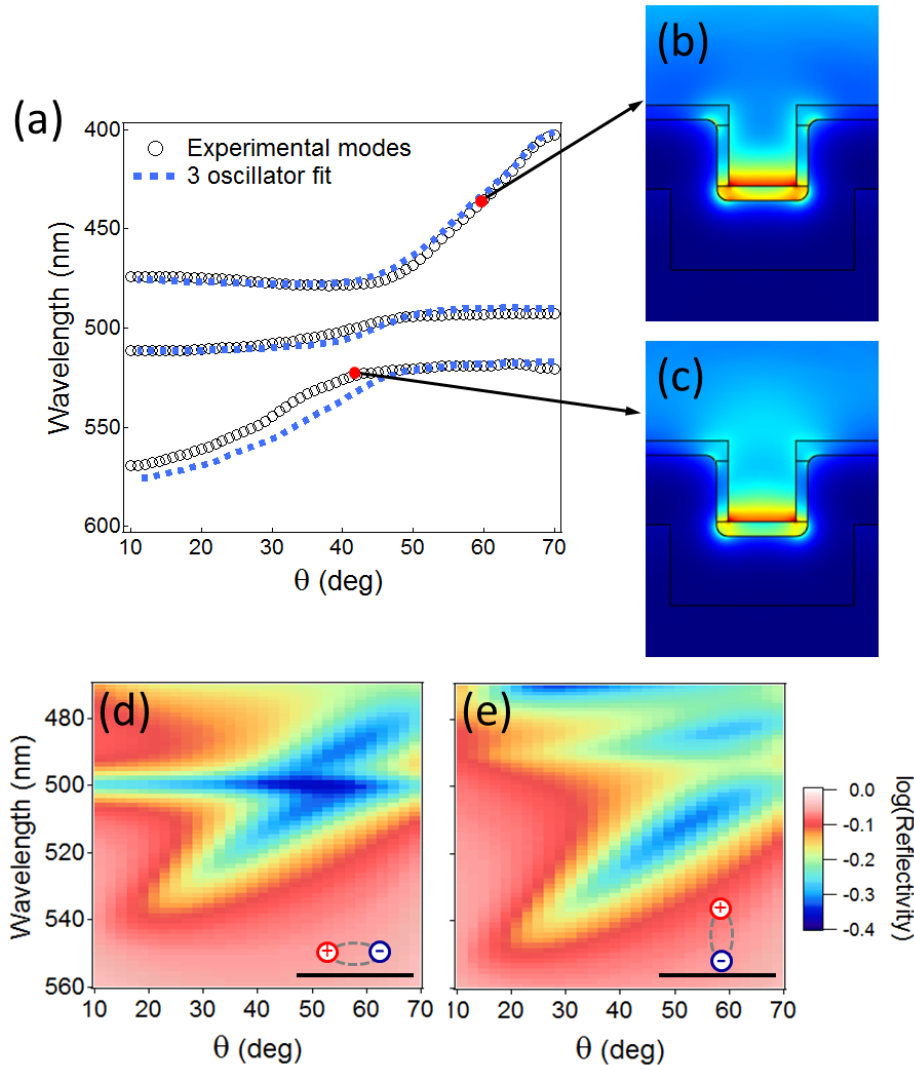


Fig. 7.18 (a) Extracted spectral mode positions for  $\phi = 90^\circ$  reflection dips (open circles), and fit from three oscillator coupling model (dashed lines). (b,c) Time-averaged  $\vec{E}$  field intensity profiles ( $\vec{E} \cdot \vec{E}$ ) as indicated. (d,e) Simulated reflection spectra for (d) in-plane and (e) out-of-plane exciton dipoles.

We calculate the full eigenstates of the system using FEM simulations. These confirm the anticrossings observed, and provide the optical field profiles. In the case of strong coupling at  $\phi = 90^\circ$ , the time-averaged near-field shows strongest intensity inside the CHPI which coats the bottom surface of the grating, with a rapid evanescent decay away from the interface [Figs. 7.18(b,c)]. The mode is thus both laterally confined by the grating as well as being trapped inside the surface layers where it couples to the excitons.

The SPP  $\vec{E}$  field direction is primarily perpendicular to the metal-dielectric interface,

while excitons in CHPI QWs are polarised parallel to this interface<sup>43,66</sup>. Simulated  $\phi = 90^\circ$  spectra for in- and out-of-plane exciton dipoles are shown in Figs. 7.18(d,e) respectively. While strong coupling is seen for both dipole orientations, the bare exciton is only seen for the in-plane dipole. It thus appears that the coupling between the excitons and their images are responsible for mixing the dipole orientations, enabling the strong coupling with the SPP mode. Far-field light is directly coupled into the layered perovskite system, where the excitons mediate SPP interactions. The polariton states mix excitons within the perovskite which are delocalised across many PbI monolayers, with SPPs which are tightly confined to the CHPI layer above the Ag grating and laterally localised in the grating slits by the coupling of standing waves. Such light-matter polaritonic quasiparticles thus combine organic, inorganic and plasmonic components in an unusual fashion.

## 7.5 Conclusions

Simple plasmonic periodic structures give rise to a wide range of grating modes: photonic modes due to the interference of light, excitation of SPPs on the surface of the metal, and laterally localised modes such as channel plasmons or waveguide modes. The positions and efficiencies of many of these modes are sensitive to the geometry of the grating and the dielectric environment provided by any overcoating materials.

In CHPI-coated Ag gratings, we observe evidence of image-biexcitons with binding energy 100 meV at room temperature. Such quasiparticles arise from the interaction between excitons and their images in the metal, and are outcoupled from the grating structure via SPP emission. These out-of-plane biexciton states mediate coupling between in-plane QW excitons and out-of-plane SPP grating modes. This enables the observation of strong coupling at room temperature with Rabi splittings of 150 and 125 meV for the exciton and image-biexciton respectively. Both the biexciton binding energy and strong coupling Rabi splitting is tunable by small changes in the structure of the coated gratings.

Strong coupling has previously been observed between inorganic or organic excitons and Au nanoslitr gratings at low temperature. The coupling constants in these systems are much smaller compared to CHPI at room temperature: 55 meV for 50 nm J-aggregate films at 77 K<sup>213</sup>, and 8 meV for 10 nm GaAs QWs at 10 K<sup>214</sup>. One key difference is that for the III-V semiconductors the QWs have to be spaced at least 20 nm from the metal surface to maintain their optical quality. In contrast our 25 nm thick CHPI film is prepared directly on the metal, and still gives strongly radiative exciton modes because the organic sandwich protects the PbI QW layers. Theoretically Fig. 7.16(a) shows that excitons remain radiative

via SPP coupling for film thickness above 10 nm. Hence the perovskite system is well suited to manipulate light-matter interactions. Such modification of exciton behaviour is of great interest for other layered van der Waals semiconductors such as derivatives of graphene and transition metal dichalcogenides, particularly for future optoelectronic devices that demand large field enhancements by coupling to SPPs.



# References

- [1] M. Faraday, *Experimental Researches in Electricity, Volume 1* (Cambridge University Press, 2012).
- [2] A. Becquerel, Comptes Rendus de l'Académie des Sciences **9**, 711 (1839).
- [3] C. Fritts, American Journal of Science **26**, 465 (1883).
- [4] W. Smith, Nature **7**, 303 (1873).
- [5] W. Adams and R. Day, Proceedings of the Royal Society A **25**, 113 (1876).
- [6] H. Round, Electrical World **49**, 309 (1907).
- [7] A. Wilson, Proceedings of the Royal Society A **133**, 458 (1931).
- [8] T. Jenkins, Physics Education **40**, 430 (2005).
- [9] URL <http://www.todaysengineer.org/2003/May/history.asp>, accessed September 2014.
- [10] C. Kittel, *Introduction to solid state physics* (John Wiley & Sons, 1986), 6th ed.
- [11] URL [http://www.beatriceco.com/bti/porticus/bell/belllabs\\_transistor.html](http://www.beatriceco.com/bti/porticus/bell/belllabs_transistor.html), accessed September 2014.
- [12] URL [http://www.greenrhinoenergy.com/solar/technologies/pv\\_manufacturing.php](http://www.greenrhinoenergy.com/solar/technologies/pv_manufacturing.php), accessed June 2014.
- [13] L. Miozzo, A. Yassar, and G. Horowitz, Journal of Materials Chemistry **20**, 2513 (2010).
- [14] URL <http://www.samsung.com/us/video/tvs/KN55S9CAFXZA>, accessed June 2014.
- [15] URL <http://www.leb.eei.uni-erlangen.de/winterakademie/2010/report/content/course03/pdf/0313.pdf>, accessed September 2014.
- [16] H. Naarmann, Ullmann's Encyclopedia of Industrial Chemistry **29**, 295 (2002).
- [17] J. Halls, K. Pichler, R. Friend, S. Moratti, and A. Holmes, Applied Physics Letters **68**, 3120 (1996).
- [18] S. Chiu, L. Lin, H. Lin, Y. Chen, Z. Huang, Y. Lin, F. Lin, Y. Liu, and K. Wong, Chemical Communications **48**, 1857 (2012).

- [19] B. Li, L. Wang, B. Kang, P. Wang, and Y. Qiu, *Solar Energy Materials & Solar Cells* **90**, 549 (2006).
- [20] H. Kaluk, *Chemical Society Reviews* **39**, 2643 (2010).
- [21] K. Fukuda, Y. Takeda, M. Mizukami, D. Kumaki, and S. Tokito, *Scientific Reports* **4**, 3947 (2014).
- [22] Y. Yuan, G. Giri, A. Ayzner, A. Zoombelt, S. Mannsfeld, J. Chen, D. Nordlund, T. MF, J. Huang, and Z. Bao, *Nature Communications* **5**, 3005 (2014).
- [23] C. Tang and S. VanSlyke, *Applied Physics Letters* **51**, 913 (1987).
- [24] J. Burroughes, D. Bradley, A. Brown, R. Marks, K. MacKay, R. Friend, P. Burns, and A. Holmes, *Nature* **347**, 539 (1990).
- [25] T. Hebner, C. Wu, D. Marcy, M. Lu, and J. Sturm, *Applied Physics Letters* **72**, 519 (1998).
- [26] Z. Cheng and J. Lin, *CrystEngComm* **12**, 2646 (2010).
- [27] T. Ishihara, J. Takahashi, and T. Goto, *Physical Review B* **42**, 11099 (1990).
- [28] D. B. Mitzi, K. Chondroudis, and C. R. Kagan, *IBM Journal of Research and Development* **45**, 29 (2001).
- [29] D. B. Mitzi and P. Brock, *Inorganic Chemistry* **40**, 2096 (2001).
- [30] A. Nagami, K. Okamura, and T. Ishihara, *Physica B: Condensed Matter* **227**, 346 (1996).
- [31] K. Pradeesh, M. Agarwal, K. K. Rao, and G. V. Prakash, *Solid State Sciences* **12**, 95 (2010).
- [32] K. Pradeesh, J. J. Baumberg, and G. V. Prakash, *Applied Physics Letters* **95**, 33309 (2009).
- [33] M. M. Lee, J. Teuscher, T. Miyasaka, T. N. Murakami, and H. J. Snaith, *Science* **338**, 643 (2012).
- [34] J. H. Heo, S. H. Im, J. H. Noh, T. N. Mandal, C. S. Lim, J. A. Chang, Y. H. Lee, H. J. Kim, A. Sarkar, M. K. Nazeeruddin, et al., *Nature Photonics* **7**, 486 (2013).
- [35] M. Liu, M. B. Johnston, and H. J. Snaith, *Nature* **501**, 395 (2013).
- [36] F. Hao, C. C. Stoumpos, D. H. Cao, R. P. H. Chang, and M. G. Kanatzidis, *Nature Photonics* **8**, 489 (2014).
- [37] T. Fujita, Y. Sato, T. Kuitani, and T. Ishihara, *Physical Review B* **57**, 12428 (1998).
- [38] T. Fujita and T. Ishihara, *Journal of the Physics Society Japan* **68**, 2918 (1999).
- [39] T. Fujita and H. Nakashima, *Physica Status Solidi (B)* **147**, 147 (2000).

- [40] J. Ishi-Hayase and T. Ishihara, Semiconductor Science and Technology **18**, S411 (2003).
- [41] A. Brehier, R. Parashkov, J. S. Lauret, and E. Deleporte, Applied Physics Letters **89**, 171110 (2006).
- [42] G. Lanty, A. Bréhier, R. Parashkov, J. S. Lauret, and E. Deleporte, New Journal of Physics **10**, 065007 (2008).
- [43] K. Pradeesh, J. J. Baumberg, and G. V. Prakash, Optics express **17**, 22171 (2009).
- [44] K. Sumioka, H. Nagahama, and T. Tsutsui, Applied Physics Letters **78**, 1328 (2001).
- [45] S. A. Vaganov, D. a. Zaitsev, and R. P. Seisyan, Technical Physics **58**, 1039 (2013).
- [46] P. Bassu, *Theory of optical processes in semiconductors: bulk and microstructures* (Oxford University Press, 1997).
- [47] T. Dammak and M. Koubaa, The Journal of Physical Chemistry C **113**, 19305 (2009).
- [48] R. Dingle, W. Wiegmann, and C. Henry, Physical Review Letters **33**, 827 (1974).
- [49] T. Fukumoto, M. Hirasawa, and T. Ishihara, Journal of Luminescence **87-89**, 497 (2000).
- [50] J. Fujisawa and T. Ishihara, Physical Review B **70**, 113203 (2004).
- [51] T. Ishihara, Journal of Luminescence **60-61**, 269 (1994).
- [52] T. Ishihara, J. Takahashi, and T. Goto, Solid State Communications **69**, 933 (1989).
- [53] G. Mousdis, G. Papavassiliou, C. Raptopoulou, and A. Terzis, Journal of Materials Chemistry **10**, 515 (2000).
- [54] D. B. Mitzi, Journal of the Chemical Society, Dalton Transactions pp. 1–12 (2001).
- [55] D. G. Billing and A. Lemmerer, CrystEngComm **8**, 686 (2006).
- [56] D. G. Billing and A. Lemmerer, New Journal of Chemistry **32**, 1736 (2008).
- [57] S. Zhang, G. Lanty, J. S. Lauret, E. Deleporte, P. Audebert, and L. Galmiche, Acta Materialia **57**, 3301 (2009).
- [58] K. Teshima, M. Suzuki, Y. Shirai, M. Rikukawa, and K. Sanui, Japanese Journal of Applied Physics **42**, L698 (2003).
- [59] K. Kikuchi, Y. Takeoka, M. Rikukawa, and K. Sanui, Colloids and Surfaces A: Physicochemical and Engineering Aspects **257-258**, 199 (2005).
- [60] Y. Kawabata, M. Yoshizawa-Fujita, Y. Takeoka, and M. Rikukawa, Synthetic Metals **159**, 776 (2009).
- [61] J. Calabrese, N. L. Jones, R. L. Harlow, N. Herron, D. L. Thorn, and Y. Wang, Journal of the American Chemical Society **113**, 2328 (1991).

- [62] S. Barman, N. V. Venkataraman, S. Vasudevan, and R. Seshadri, *Journal of Physical Chemistry B* **107**, 1875 (2003).
- [63] C. Xu, S. Fukuta, T. Kondo, R. Ito, Y. Takahashi, and K. Kumata, *Solid State Communications* **77**, 923 (1991).
- [64] V. V. Naik and S. Vasudevan, *Journal of Physical Chemistry C* **4**, 4536 (2010).
- [65] K. Pradeesh, J. J. Baumberg, and G. V. Prakash, *Applied Physics Letters* **95**, 173305 (2009).
- [66] D. B. Mitzi, *Chemistry of Materials* **13**, 3283 (2001).
- [67] N. Kitazawa, *Japanese Journal of Applied Physics* **35**, 6202 (1996).
- [68] Z. Tang, J. Guan, and A. M. Guloy, *Journal of Materials Chemistry* **293**, 479 (2001).
- [69] X. Hong, T. Ishihara, and A. V. Nurmikko, *Solid State Communications* **84**, 657 (1992).
- [70] Z. Cheng, H. Wang, Z. Quan, C. Lin, J. Lin, and Y. Han, *Journal of Crystal Growth* **285**, 352 (2005).
- [71] P. Audebert, G. Clavier, V. Alain-Rizzo, E. Deleporte, S. Zhang, J. Lauret, G. Lanty, and C. Boissiere, *Chemistry of Materials* **21**, 210 (2009).
- [72] M. Era and S. Oka, *Thin Solid Films* **376**, 232 (2000).
- [73] K. Liang, D. D. B. D. Mitzi, and M. M. M. T. Prikas, *Chemistry of Materials* **4756**, 403 (1998).
- [74] T. Matsui, A. Yamaguchi, Y. Takeoka, M. Rikukawa, and K. Sanui, *Chemical Communications* **3**, 1094 (2002).
- [75] M. Era and K. Maeda, *Thin Solid Films* **331**, 285 (1998).
- [76] S. Ahmad, P. Kanaujia, W. Niu, J. Baumberg, and G. Vijaya Prakash, *ACS Applied Materials & Interfaces* **6**, 10238 (2014).
- [77] M. Era and T. Hattori, *Chemistry of Materials* **9**, 8 (1997).
- [78] D. B. Mitzi, M. T. Prikas, and K. Chondroudis, *Chemistry of Materials* **11**, 542 (1999).
- [79] K. Chondroudis, D. B. Mitzi, and P. Brock, *Chemistry of Materials* **12**, 169 (2000).
- [80] T. Kataoka, T. Kondo, R. Ito, S. Sasaki, K. Uchida, and N. Miura, *Physica B* **201**, 423 (1994).
- [81] G. Vijaya Prakash, K. Pradeesh, R. Ratnani, K. Saraswat, M. E. Light, and J. J. Baumberg, *Journal of Physics D: Applied Physics* **42**, 185405 (2009).
- [82] T. Kataoka, T. Kondo, and R. Ito, *Physical Review B* **47**, 2010 (1993).
- [83] N. Kitazawa, *Journal of Materials Science* **3**, 5 (1998).

- [84] Y. Wei, P. Audebert, L. Galmiche, J.-S. Lauret, and E. Deleporte, *Materials* **7**, 4789 (2014).
- [85] N. Kitazawa and Y. Watanabe, *Journal of Materials Science* **37**, 4845 (2002).
- [86] Z. Y. Cheng, Z. Wang, R. B. Xing, Y. C. Han, and J. Lin, *Chemical Physics Letters* **376**, 481 (2003).
- [87] T. Umebayashi, K. Asai, T. Kondo, and A. Nakao, *Physical Review B* **67**, 2 (2003).
- [88] K. Matsuishi, T. Ishihara, S. Onari, Y. H. Chang, and C. H. Park, *Physica Status Solidi (B)* **241**, 3328 (2004).
- [89] T. Kondo, M. Mizuno, S. Iwamoto, S. Hayase, K. Tanaka, J. Ishi, K. Ema, and R. Ito, *Solid State Communications* **105**, 503 (1998).
- [90] T. Goto, N. Ohshima, G. A. Mousdis, and G. C. Papavassiliou, *Solid State Communications* **117**, 13 (2001).
- [91] N. Kitazawa, *Materials Science and Engineering B* **49**, 233 (1997).
- [92] S. Ahmad, J. J. Baumberg, and G. Vijaya Prakash, *Journal of Applied Physics* **114**, 233511 (2013).
- [93] C. Xu, H. Sakakura, T. Kondo, S. Takeyama, N. Miura, Y. Takahashi, K. Kumata, and R. Ito, *Solid State Communications* **79**, 249 (1991).
- [94] K. Tanaka, F. Sano, T. Takahashi, T. Kondo, R. Ito, and K. Ema, *Solid State Communications* **122**, 249 (2002).
- [95] T. Kondo, T. Azuma, T. Yuasa, and R. Ito, *Solid State Communications* **105**, 253 (1998).
- [96] M. Shimizu, J. Fujisawa, and T. Ishihara, *Physical Review B* **74** (2006).
- [97] T. Ishihara, X. Hong, J. Ding, and A. Nurmikko, *Surface Science* **267**, 323 (1992).
- [98] M. Kumagai and T. Takagahara, *Physical Review B* **40**, 12359 (1989).
- [99] M. Hirasawa, T. Ishihara, and T. Goto, *Journal of the Physical Society of Japan* **63**, 3870 (1994).
- [100] M. Shinada and S. Sugano, *Journal of the Physical Society of Japan* **21**, 1936 (1966).
- [101] E. Muljarov, S. Tikhodeev, and N. Gippius, *Physical Review B* **51**, 14370 (1995).
- [102] S. Sourisseau, N. Louvain, W. Bi, N. Mercier, D. Rondeau, F. Boucher, J. Y. Buzaré, and C. Legein, *Chemistry of Materials* **19**, 600 (2007).
- [103] J. L. Knutson, J. D. Martin, and D. B. Mitzi, *Inorganic Chemistry* **44**, 4699 (2005).
- [104] K. Matsuishi, T. Suzuki, S. Onari, E. Gregortanz, R. J. Hemley, and H. K. Mao, *Physica Status Solidi (B)* **223**, 177 (2001).

- [105] N. Mercier, S. Poiroux, A. Riou, and P. Batail, Inorganic Chemistry **43**, 8361 (2004).
- [106] D. B. Mitzi, K. Chondroudis, and C. R. Kagan, Inorganic Chemistry **38**, 6246 (1999).
- [107] M. Braun, Chemical Physics Letters **303**, 157 (1999).
- [108] J. Kasprzak, M. Richard, S. Kundermann, a. Baas, P. Jeambrun, J. M. J. Keeling, F. M. Marchetti, M. H. Szymańska, R. André, J. L. Staehli, et al., Nature **443**, 409 (2006).
- [109] S. Christopoulos, G. von Högersthal, A. Grundy, P. Lagoudakis, A. Kavokin, J. Baumberg, G. Christmann, R. Butté, E. Feltin, J. Carlin, et al., Physical Review Letters **98**, 126405 (2007).
- [110] A. Amo, T. C. H. Liew, C. Adrados, R. Houtré, E. Giacobino, A. V. Kavokin, and A. Bramati, Nature Photonics **4**, 361 (2010).
- [111] M. Era, S. Morimoto, T. Tsutsui, and S. Saito, Applied Physics Letters **65**, 676 (1994).
- [112] T. Matsushima, K. Fujita, and T. Tsutsui, Japanese Journal of Applied Physics **44**, 1457 (2005).
- [113] T. Hattori, T. Taira, M. Era, T. Tsutsui, and S. Saito, Chemical Physics Letters **254**, 103 (1996).
- [114] D. B. Mitzi, C. A. Felid, W. T. A. Harrison, and M. Guloy, A, Nature **369**, 467 (1994).
- [115] D. Mitzi, C. Dimitrakopoulos, and L. Kosbar, Device Research **467**, 185 (2002).
- [116] D. B. Mitzi, C. D. Dimitrakopoulos, and L. L. Kosbar, Chemistry of Materials **13**, 3728 (2001).
- [117] C. R. Kagan, Science **286**, 945 (1999).
- [118] K. Shibuya, M. Koshimizu, Y. Takeoka, and K. Asai, Nuclear Instruments and Methods in Physics Research B **194**, 207 (2002).
- [119] S. Kengo, K. Masanori, S. Hiromi, and A. Keisuke, Proceedings of IEEE Sensors **1**, 552 (2002).
- [120] K. Shibuya, M. Koshimizu, H. Murakami, Y. Muroya, Y. Katsumura, and K. Asai, Japanese Journal of Applied Physics **43**, L1333 (2004).
- [121] E. J. Zeman and G. C. Schatz, Journal of Physical Chemistry **91**, 634 (1987).
- [122] P. Johnson and R. Christy, Physical Review B **6**, 4370 (1972).
- [123] S. Maier, *Plasmonics: Fundamentals and Applications* (Springer, 2007).
- [124] Y. Chen, E. Koteles, R. Seymour, G. Sonek, and J. Ballantyne, Solid State Communications **46**, 95 (1983).
- [125] M. Hutley and D. Maystre, Optics Communications **19**, 431 (1976).
- [126] R. Wood, Proceedings of the Physical Society **18**, 396 (1902).

- [127] U. Fano, Journal of the Optical Society of America **31**, 213 (1941).
- [128] A. Hessel and A. Oliner, Applied Optics **4**, 1275 (1965).
- [129] K. Lee and Q. H. Park, Physical Review Letters **95**, 103902 (2005).
- [130] H. Lochbihler, Physical Review B **50**, 4795 (1994).
- [131] R. Ritchie, E. Arakawa, J. Cowan, and R. Hamm, Physical Review Letters **21**, 1530 (1968).
- [132] M. Treacy, Physical Review B **66**, 195105 (2002).
- [133] R. Watts, T. Preist, and J. Sambles, Physical Review Letters **79**, 3978 (1997).
- [134] M. Hutley, *Diffraction gratings* (Academic Press Inc. Ltd., 1982).
- [135] E. Loewen and E. Popov, *Diffraction gratings and applications* (Marcel Dekker, Inc., 1997).
- [136] J. Jackson, *Classical electrodynamics* (Wiley, 1999), 3rd ed.
- [137] S. Bozhevolnyi, V. Volkov, E. Devaux, and T. Ebbesen, Physical Review Letters **95**, 1 (2005).
- [138] T. Srivastava and A. Kumar, Journal of Applied Physics **106**, 043104 (2009).
- [139] S. Chattopadhyay and P. K. Saha, ISRN Optics **2012**, 1 (2012).
- [140] I. Novikov and A. Maradudin, Physical Review B **66**, 1 (2002).
- [141] M. Kuttge, F. J. G. de Abajo, and A. Polman, Optics Express **17**, 10385 (2009).
- [142] T. Sondergaard, S. M. Novikov, T. Holmgård, R. L. Eriksen, J. Beermann, Z. Han, K. Pedersen, and S. I. Bozhevolnyi, Nature Communications **3**, 969 (2012).
- [143] W. Rechberger, A. Hohenau, A. Leitner, J. Krenn, B. Lamprecht, and F. Aussenegg, Optics Communications **220**, 137 (2003).
- [144] M. Born and E. Wolf, *Principles of Optics: Electromagnetic theory of propagation, interference and diffraction of light* (Cambridge University Press, 1999), 7th ed.
- [145] B. Wiley, S. Im, and Z. Li, The Journal of Physical Chemistry B **110**, 15666 (2006).
- [146] B. J. Wiley, Y. Chen, J. M. McLellan, Y. Xiong, Z. Y. Li, D. Ginger, and Y. Xia, Nano Letters **7**, 1032 (2007).
- [147] H. Chen, L. Shao, Q. Li, and J. Wang, Chemical Society Reviews **42**, 2679 (2013).
- [148] D. Meyerhofer, Journal of Applied Physics **49**, 3993 (1978).
- [149] R. van Hardeveld, P. Gunter, L. van IJzenddorn, W. Wieldraaijer, E. Kuipers, and J. Niemantsverdriet, Applied Surface Science **84**, 339 (1995).

- [150] C. J. Lawrence, Physics of Fluids **31**, 2786 (1988).
- [151] D. P. Birnie, S. K. Hau, D. S. Kamber, and D. M. Kaz, Journal of Materials Science: Materials in Electronics **16**, 715 (2005).
- [152] URL <http://www.co2clean.com/clnmech.htm>, accessed May 2014.
- [153] K. S. Novoselov, A. K. Geim, S. V. Morozov, D. Jiang, Y. Zhang, S. V. Dubonos, I. V. Grigorieva, and A. A. Firsov, Science **306**, 666 (2004).
- [154] P. Blake, E. W. Hill, A. H. Castro Neto, K. S. Novoselov, D. Jiang, R. Yang, T. J. Booth, and A. K. Geim, Applied Physics Letters **91**, 063124 (2007).
- [155] Z. H. Ni, H. M. Wang, J. Kasim, H. M. Fan, T. Yu, Y. H. Wu, Y. P. Feng, and Z. X. Shen, Nano letters **7**, 2758 (2007).
- [156] A. Splendiani, L. Sun, Y. Zhang, T. Li, J. Kim, C. Y. Chim, G. Galli, and F. Wang, Nano Letters **10**, 1271 (2010).
- [157] A. Castellanos-Gomez, N. Agrait, and G. Rubio-Bollinger, Applied Physics Letters **96**, 213116 (2010).
- [158] P. Tonndorf, R. Schmidt, P. Bottger, X. Zhang, J. Borner, A. Liebig, M. Albrecht, C. Kloc, O. Gordan, D. Zahn, et al., Optics Express **21**, 4908 (2013).
- [159] I. Saikumar, S. Ahmad, J. J. Baumberg, and G. Vijaya Prakash, Scripta Materialia **67**, 834 (2012).
- [160] D. G. Billing and A. Lemmerer, Acta crystallographica. Section C, Crystal structure communications **62**, m269 (2006).
- [161] J. Fujisawa and N. Tajima, Physical Review B **72**, 125201 (2005).
- [162] J. Fujisawa, N. Tajima, K. Tamaki, M. Shimomura, and T. Ishihara, Journal of Physical Chemistry C **111**, 1146 (2007).
- [163] S. Zhang, P. Audebert, Y. Wei, A. Al Choueiry, G. Lanty, A. Bréhier, L. Galmiche, G. Clavier, C. Boissière, J. S. Lauret, et al., Materials **3**, 3385 (2010).
- [164] S. Baranovskii, U. Doerr, and P. Thomas, Physical Review B **48**, 17149 (1993).
- [165] L. Andreani and G. Panzarini, Physical Review B **57**, 4670 (1998).
- [166] I. Kuznetsova, N. Gogh, J. Förstner, T. Meier, S. T. Cundiff, I. Varga, and P. Thomas, Physical Review B **81**, 075307 (2010).
- [167] T. Iwasaki, T. Goto, and Y. Nishina, Physica Status Solidi (B) **88**, 289 (1978).
- [168] T. Goto and J. Maeda, Journal of the Physical Society of Japan **56**, 3710 (1987).
- [169] T. Jensen, M. Malinsky, C. Haynes, and R. Van Duyne, The Journal of Physical Chemistry B **104**, 10549 (2000).

- [170] G. Xu, M. Tazawa, P. Jin, and S. Nakao, *Applied Physics A* **80**, 1535 (2004).
- [171] M. Malinsky, K. Kelly, G. Schatz, and R. Van Duyne, *The Journal of Physical Chemistry B* **105**, 2343 (2001).
- [172] P. Royer, J. Goudonnet, R. Warmack, and T. Ferrell, *Physical Review B* **35**, 3753 (1987).
- [173] N. Cade, T. Ritman-Meer, and D. Richards, *Physical Review B* **79**, 241404 (2009).
- [174] L. G. Olson, Y. S. Lo, T. P. Beebe, and J. M. Harris, *Analytical chemistry* **73**, 4268 (2001).
- [175] C. E. Talley, J. B. Jackson, C. Oubre, N. K. Grady, C. W. Hollars, S. M. Lane, T. R. Huser, P. Nordlander, and N. J. Halas, *Nano letters* **5**, 1569 (2005).
- [176] R. Toftegaard, J. Arnbjerg, H. Cong, H. Agheli, D. S. Sutherland, and P. R. Ogilby, *Pure and Applied Chemistry* **83**, 885 (2011).
- [177] C. Y. Cho, M. K. Kwon, S. J. Lee, S. H. Han, J. W. Kang, S. E. Kang, D. Y. Lee, and S. J. Park, *Nanotechnology* **21**, 205201 (2010).
- [178] V. Reboud, G. Lévéque, M. Striccoli, T. Placido, A. Panniello, M. L. Curri, J. A. Alducin, T. Kehoe, N. Kehagias, D. Mecerreyes, et al., *Nanoscale* **5**, 239 (2013).
- [179] L. Blanco and F. García de Abajo, *Journal of Quantitative Spectroscopy and Radiative Transfer* **89**, 37 (2004).
- [180] N. Kaiser, *Applied Optics* **41**, 3053 (2002).
- [181] R. S. Sennett and G. D. Scott, *Journal of the Optical Society of America* **40**, 203 (1950).
- [182] R. Gupta, M. J. Dyer, and W. A. Weimer, *Journal of Applied Physics* **92**, 5264 (2002).
- [183] H. Walter, G. Bauer, R. Domnick, G. Jakopic, and A. Leitner, *Optical Engineering* **45**, 103801 (2006).
- [184] P. Gadenne and J. C. Rivoal, *Topics in Applied Physics* **82**, 185 (2002).
- [185] M. M. Lee, P. P. Dobson, and B. Cantor, *Thin Solid Films* **219**, 199 (1992).
- [186] S. Yamaguchi, *Journal of the Physical Society of Japan* **15**, 1577 (1960).
- [187] T. Yamaguchi, S. Yoshida, and A. Kinbara, *Thin Solid Films* **13**, 261 (1972).
- [188] T. Yamaguchi, S. Yoshida, and A. Kinbara, *Thin Solid Films* **18**, 63 (1973).
- [189] R. H. Doremus, *Journal of Applied Physics* **37**, 2775 (1966).
- [190] S. Balci, E. Karademir, C. Kocabas, and A. Aydinli, *Optics Letters* **39**, 4994 (2014).
- [191] N. Alemu and F. Chen, *Physica Status Solidi (a)* **211**, 213 (2014).

- [192] Y. Zheng, B. Kiraly, and S. Cheunkar, *Nano Letters* **11**, 2061 (2011).
- [193] Q. Xu, F. Liu, Y. Liu, K. Cui, X. Feng, W. Zhang, and Y. Huang, *Scientific Reportseports* **3**, 2112 (2013).
- [194] P. Spinelli and A. Polman, *Optics Express* **20**, 205 (2012).
- [195] C. Haynes and R. V. Duyne, *The Journal of Physical Chemistry B* **105**, 5599 (2001).
- [196] J. Hulteen and R. V. Duyne, *Journal of Vacuum Science & Technology A* **13**, 1553 (1995).
- [197] J. C. Hulteen, D. A. Treichel, M. T. Smith, M. L. Duval, T. R. Jensen, and R. P. van Duyne, *The Journal of Physical Chemistry B* **103**, 3854 (1999).
- [198] C. L. Haynes, A. D. McFarland, M. T. Smith, J. C. Hulteen, and R. P. Van Duyne, *The Journal of Physical Chemistry B* **106**, 1898 (2002).
- [199] T. Jensen, G. Schatz, and R. Van Duyne, *The Journal of Physical Chemistry B* **103**, 2394 (1999).
- [200] R. French, J. Rodríguez-Parada, M. Yang, R. Derryberry, and N. Pfeiffenberger, *Solar Energy Materials and Solar Cells* **95**, 2077 (2011).
- [201] H. Morawitz, *Physical Review* **187**, 1792 (1969).
- [202] H. Morawitz and M. Philpott, *Physical Review B* **10**, 4863 (1974).
- [203] R. R. Chance, A. Prock, and R. Silbey, *The Journal of Chemical Physics* **60**, 2184 (1974).
- [204] R. R. Chance, A. Prock, and R. Silbey, *Physical Review A* **12**, 1448 (1975).
- [205] R. R. Chance, A. Prock, and R. Silbey, *The Journal of Chemical Physics* **62**, 2245 (1975).
- [206] G. Ford and W. Weber, *Physics Reports* **113**, 195 (1984).
- [207] J. Frischeisen, Q. Niu, A. Abdellah, J. B. Kinzel, R. Gehlhaar, G. Scarpa, C. Adachi, P. Lugli, and W. Brütting, *Optics Express* **S1**, A7 (19).
- [208] A. Kumar, R. Srivastava, P. Tyagi, D. Mehta, and M. Kamalasan, *Organic Electronics* **13**, 159 (2012).
- [209] R. Tamaki, Y. Arai, D. Ichikawa, M. Inoue, H. Kunugita, and K. Ema, *Journal of Luminescence* **128**, 842 (2008).
- [210] J. Baumberg, A. Heberle, A. Kavokin, M. Vladimirova, and K. Köhler, *Physical Review Letters* **80**, 3567 (1998).
- [211] A. Kavokin and J. Baumberg, *Physical Review B* **57**, 12697 (1998).
- [212] M. Vladimirova, E. Ivchenko, and A. Kavokin, *Semiconductors* **32**, 90 (1998).

- [213] P. Vasa, R. Pomraenke, G. Cirmi, E. De Re, W. Wang, S. Schwieger, D. Leipold, E. Runge, G. Cerullo, and C. Lienau, ACS Nano **4**, 7559 (2010).
- [214] P. Vasa, R. Pomraenke, S. Schwieger, Y. Y. I. Mazur, V. Kunets, P. Srinivasan, E. Johnson, J. Kihm, D. Kim, E. Runge, et al., Physical Review Letters **101**, 116801 (2008).